

# WOODS: BENCHMARKS FOR OUT-OF-DISTRIBUTION GENERALIZATION IN TIME SERIES TASKS

---

**Jean-Christophe Gagnon-Audet**

Mila - Québec AI Institute  
Université of Montréal

jean-christophe.gagnon-audet@mila.quebec

**Kartik Ahuja**

Mila - Québec AI Institute  
Université of Montréal

**Mohammad-Javad Darvishi-Bayazi**

Mila - Québec AI Institute  
Université of Montréal

**Guillaume Dumas**

Mila - Québec AI Institute  
CHU Sainte-Justine Research Center, Department of Psychiatry  
Université of Montréal

**Irina Rish**

Mila - Québec AI Institute  
Université of Montréal

## ABSTRACT

Machine learning models often fail to generalize well under distributional shifts. Understanding and overcoming these failures have led to a research field of Out-of-Distribution (OOD) generalization. Despite being extensively studied for static computer vision tasks, OOD generalization has been underexplored for time series tasks. To shine light on this gap, we present WOODS: eight challenging open-source time series benchmarks covering a diverse range of data modalities, such as videos, brain recordings, and sensor signals. We revise the existing OOD generalization algorithms for time series tasks and evaluate them using our systematic framework. Our experiments show a large room for improvement for empirical risk minimization and OOD generalization algorithms on our datasets, thus underscoring the new challenges posed by time series tasks. Code and documentation are available at <https://woods-benchmarks.github.io/>

## 1 Introduction

In the last decade, the success of deep learning has led to impactful applications spanning many fields [53, 111, 100, 46, 14]. However, parallel to this surge, there is growing evidence that deep learning models exploit undesired correlations appearing due to selection biases, confounding factors, and other biases in the data [26, 99, 121]. These biases can often lead to shortcuts that help the model arrive at low empirical risk on a dataset. Nevertheless, a prediction rule relying on these shortcuts will not generalize out of its training distribution as they rely on correlation instead of causation [84, 95]. Such a failure becomes very concerning in real-life applications that directly impact human lives, such as medicine [81, 18, 79] or self-driving cars [7, 43].

Let us explain a concrete example of this failure with a common example from the work of Beery et al. [11]. Consider the task of distinguishing cows and camels in pictures. We train a deep learning model to minimize the empirical risk on a labeled dataset. However, the dataset is heavily tainted by selection bias, as the vast majority of cow images were taken in green pastures, and the vast majority of camel images were taken in sandy areas. At test time, we observe that our deep learning model consistently and confidently classifies images of cows on sandy beaches as camels. We conclude that the model successfully minimized the empirical risk over the training dataset by leveraging the selection bias, thus classifying green backgrounds as cows and beige backgrounds as camels.

As a way to capture this failure of deep learning models, much work has gone into finding and standardizing datasets with distributional shifts [29, 122, 51]. These datasets provide a direction for research efforts in the field of OOD

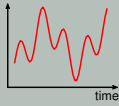






	Spurious Fourier	Temporal CMNIST	CAP	SEDFx	PCL	LSA64	HHAR
Modality	Signal	Video	EEG	EEG	EEG	Video	Sensors
Inputs							
Prediction	Frequency Peak	Parity of Sum	Sleep Stage	Sleep Stage	Imagined Action	Signed Word	Activity
Domains	<div>Spurious frequency peaks correlation 90%</div> <div>Spurious frequency peaks correlation 80%</div> <div>Spurious frequency peaks correlation 10%</div>	<div>Spurious digit color correlation 90%</div> <div>Spurious digit color correlation 80%</div> <div>Spurious digit color correlation 10%</div>	<div>Machine A</div> <div>Machine B</div> <div>Machine C</div> <div>Machine D</div> <div>Machine E</div>	<div>Age 20-40</div> <div>Age 40-60</div> <div>Age 60-80</div> <div>Age 80-100</div>	<div>PhysionetMI</div> <div>Cho2017</div> <div>Lee2019_MI</div>	<div>Signer 1 &amp; 2</div> <div>Signer 3 &amp; 4</div> <div>Signer 5 &amp; 6</div> <div>Signer 7 &amp; 8</div> <div>Signer 9 &amp; 10</div>	<div>Nexus 4</div> <div>G. S3 mini</div> <div>Galaxy S3</div> <div>LG watch</div> <div>Sam. Gear</div>
	Synthetic challenge		Real-world datasets				

Figure 1: WOODS is a curated set of eight datasets targeting critical problems in various data modalities, such as video, brain recordings, and sensor signals.

generalization. Gulrajani and Lopez-Paz [29] gathered seven standard image datasets with distribution shifts and concluded that no OOD generalization algorithm considerably outperformed ERM, highlighting the need for better and more versatile solutions. Ye et al. [122] showed that some algorithms outperform ERM on specific types of shifts, highlighting that there might be “no free lunch” and that different algorithms might be needed for different shifts. Koh et al. [51] created a set of benchmarks of in-the-wild distribution shifts, highlighting the challenges in real-world applications.

The above mentioned works have led to crucial empirical and theoretical insights towards addressing the OOD generalization failure in deep learning. However, they have been predominantly focused on static computer vision tasks, leaving the field of time series severely underexplored despite being essential to various applications such as computational medicine [107, 120, 44], natural sciences [103, 105], finance [96, 34, 4], climate [68], retail [13], ecology [15, 20], energy [22] and many more [109, 61]. In this work, we take the first step towards a deeper understanding of distributional shifts in time series data with WOODS: a benchmark of eight open-source datasets targeting critical problems in various data modalities, such as videos, brain recordings, and sensor signals (See Figure 1).

Our contributions are:

- A curated benchmark of eight datasets exhibiting significant OOD generalization failures when trained with ERM [110];
- We introduce the Time-domain setting for intrasample temporal distribution shift
- We adapt standard OOD generalization algorithms to the time series setting and provide their results as baselines for future work;
- We also provide a new model selection strategy for a more pragmatic use in real-world datasets; and,
- We conclude through extensive experiments that algorithms regularizing representations of models are a promising approach to improve OOD performance on our real-world datasets.

## 2 Related works

In this section, we lay the background for this work with related works covering both OOD generalization benchmarks and existing algorithms.

### 2.1 OOD generalization algorithms

Several algorithms were recently proposed to address the OOD generalization failures of deep learning [5, 54, 77, 3, 89, 72, 97, 52, 83, 88, 80, 1, 119, 69, 62, 64, 87, 17, 98]. Most of these algorithms adopt the invariance principle from causality [74, 73, 76] to create predictors that rely on the causes of the label to make predictions. Invariance is leveraged because it is a more flexible and scalable alternative to conditional independence testing typically used for causal

discovery [124, 104]. An optimal predictor that relies on the cause will be invariant and min-max optimal [2, 69, 85] under a large class of distribution shifts.

## 2.2 Existing benchmarks for OOD generalization

This section discusses the current state of benchmarks for OOD generalization.

**Synthetic datasets** Many synthetic and semisynthetic datasets were created to gain a better understanding of generalization failure in deep learning, e.g., CMNIST [5] investigates our motivating cow or camel classification problem, RMNIST [27] investigates invariance with respect to rotation of images, and Invariance Unit Tests [6] investigates six different types of distributional shifts for linear models.

**Image datasets** Many real (i.e., non-synthetic) image datasets were proposed, some with naturally occurring distribution shifts and some with artificially induced distribution shifts. Several of these datasets are composed of different renditions of the same underlying labels, e.g., PACS [59] (Photo, Art, Cartoon, Sketch), DomainNet [75] (Clipart, Infographic, Painting, Quickdraw, Photo, Sketch), Office-Home [112] (Art, Clipart, Product, Photo), and ImageNet-R [37] (art, cartoons, graffiti, embroidery). Others focus on the generalization across different datasets with same rendition, such as many altered versions of ImageNet, e.g., ImageNet-A [38] comprises of ImageNet images that are misclassified by ResNet models, ImageNet-C [35] comprises algorithmically corrupted images from the original ImageNet, ImageNet-Sketch [113] comprises samples through Google Image queries, ImageNet-V2 [82] comprises similar images to ImageNet collected by closely following the original labeling protocol, BREEDS [91] comprises of ImageNet subclasses that are held out during training. Others created datasets of similar rendition with similarly gathered images, e.g., VLCS [108] comprises images from four different photo datasets, ObjectNet [9] comprises images from different predefined viewpoints, Terra Incognita [11] comprises images from multiple different traps. Another dataset class has strong spurious features that create shortcuts to minimize the empirical risk, e.g., CelebA [63] uses hair color as a spurious attribute to a gender classification task, while NICO [33] and Waterbirds use the background as a spurious attribute of animal classification task. Finally, some other datasets were created to study specific problems, e.g., the backgrounds challenge [118] aims to create more background-robust models, and Shift15m [50] that looks at OOD generalization in the large data regime.

**Language datasets** Natural language is prone to distribution shifts because of interindividual variability, consequently, many works investigated OOD generalization in language. The Machine Translation dataset from the work of Malinin et al. [66] investigates generalization to atypical language usage in a translation task. Csordás et al. [21] explored the systematic generalization of transformers with five datasets, i.e., SCAN [55] uses splits of different sentence lengths, CFQ [48] uses splits of different text structures, PCFG [41] uses different split definitions to investigate different aspects of generalization, COGS [49] uses splits that can be addressed with compositional generalization, and the Mathematics dataset [92] uses extrapolation sets to measure generalization. Hendrycks et al. [36] showed that pretrained transformers help OOD generalization compared to other language models. They use three sentiment analysis datasets, i.e., generalization between SST-2 [101] and IMDB [65], the Yelp Review Dataset with food types as domains, the Amazon Review Dataset [67, 32] with domains composed of clothing categories. They also used three reading comprehension datasets, i.e., STS-B [16] has text of different genres (news and captions), ReCoRD [125] has news paragraphs from different news sources (CNN and Daily Mail), and MNLI [116] has text from differently communicated interactions such as transcribed telephone and face-to-face conversations.

**Temporal datasets** Some works looked at temporal distributional shifts in different settings. In natural language processing, Lazaridou et al. [57] investigated the ability of neural language models to generalize to future utterances beyond their training period on the WMT [10] and ArXiv [114] datasets. In the clinical setting, both Zhang et al. [123] and Guo et al. [31] investigated shifts when data is grouped according to the year in which they were gathered: the former used in-hospital mortality records and X-rays of the lungs, while the later used patients health record in the ICU. Malinin et al. [66] investigated temporal shifts in large amounts of weather data.

**Other modalities** There has been efforts in studying OOD generalization on graphs, such as works from Li et al. [60] and the OGB-MolPCBA [51] dataset adapted from the Open Graph Benchmark [40].

Besides individual datasets, multiple works focused on gathering and standardizing datasets for a unified measure of OOD generalization algorithm performance. Gulrajani and Lopez-Paz [29] introduced DomainBed: a collection of seven image datasets (i.e., CMNIST, RMNIST, PACS, VLCS, Office-Home, Terra Incognita, DomainNet) for a systematic OOD performance evaluation of algorithms. Ye et al. [122] built on top of DomainBed and added three datasets (i.e., Camelyon17-WILDS, NICO, and CelebA), along with a measure to group the datasets according to their

distributional shift. Koh et al. [51] introduced WILDS: a benchmark of several new in-the-wild distribution shifts datasets across diverse data modalities, i.e., iWildCam2020-WILDS, Camelyon17-WILDS, RxRx1-WILDS, OGB-MolPCBA, GlobalWheat-WILDS, CivilComments-WILDS, FMoW-WILDS, PovertyMap-WILDS, Amazon-WILDS, and Py150-WILDS. WILDS was recently extended with unlabeled samples for multiple of its datasets [90].

### 3 Problem formulation

This section lays down the definitions of distributional shift, invariant prediction, and describes the OOD generalization objective in static and time series settings.

#### 3.1 Static tasks

Consider the standard OOD generalization setting for static supervised learning tasks. Data samples for a domain  $d$ :  $(X^d, Y^d)$  consists of the input observation  $X^d$  and the corresponding label  $Y^d$ . We gather a dataset  $D^{\text{train}}$  from a set of training domains  $\mathcal{E}_{\text{train}}$  such that  $D^{\text{train}} = \cup_{d \in \mathcal{E}_{\text{train}}} D^d$ , where  $D^d$  is the dataset from domain  $d \in \mathcal{E}_{\text{train}}$  containing  $n^d$  samples. The data from domain  $d$  follows the distribution  $\mathbb{P}^d(X, Y)$ . We define a predictor  $f : \mathcal{X} \rightarrow \mathcal{Y}$ . The performance of this predictor  $f$  on domain  $d$  is measured in terms of the risk  $R^d(f) = \mathbb{E}^d(\ell(f(X), Y))$ , where  $\mathbb{E}^d$  is the expectation over the distribution  $\mathbb{P}^d$  and  $\ell : \mathcal{Y} \times \mathcal{Y} \rightarrow \mathbb{R}_{\geq 0}$  denotes the loss function. We evaluate the predictor on a set of test domains denoted as  $\mathcal{E}_{\text{all}}$ , where  $\mathcal{E}_{\text{train}} \subseteq \mathcal{E}_{\text{all}}$ . The goal of OOD generalization is to use the training dataset  $D^{\text{train}}$  and construct a predictor  $f$  that can perform well on the test domain. We write this objective formally as follows

**Problem 3.1.** Find a predictor  $f^*$  that solves

$$\min_f \max_{d \in \mathcal{E}_{\text{all}}} R^d(f)$$

Here, some restrictions are necessary on the set of testing domain  $\mathcal{E}_{\text{all}}$  to make Problem 3.1 a meaningful problem to solve. Otherwise, without restrictions, the best a predictor can achieve is random guessing, as nothing can be assumed about the unseen domains. Commonly, we assume that *the relationship between the label and some subset of features is invariant across all domains*<sup>1</sup>. We call this subset of features the *invariant features*, and any other features that might be correlated with the label are called *spurious features*.

The predictor  $f^*$  solving Problem 3.1 is said to be *OOD-optimal* as it has learned to leverage the invariant features that generalize to all domains in  $\mathcal{E}_{\text{all}}$ . Because the set of training domains  $\mathcal{E}_{\text{train}}$  is much smaller than the set of testing domains  $\mathcal{E}_{\text{all}}$ , learning features that generalize to all test domains is a challenging task.

#### 3.2 Time series tasks

Now consider the OOD generalization setting for time series tasks. Time series tasks can be split into two settings: single prediction tasks and multiple prediction tasks.

##### 3.2.1 Single prediction tasks

Data samples for a domain  $d$ :  $(\mathbf{X}^d, Y^d) = (X_t^d, Y_t^d)_{t \in \{1, \dots, T\}}$  consist of the input time series observation  $\mathbf{X}^d$  of length  $T$  and the single corresponding label  $Y^d$  for the time series. Similar to the previous section, we gather a dataset from a set of training domains  $\mathcal{E}_{\text{train}}$  such that  $D^{\text{train}} = \cup_{d \in \mathcal{E}_{\text{train}}} D^d$ . The data from domain  $d$  follows the distribution  $\mathbb{P}^d(\mathbf{X}, Y)$ . We define a predictor  $f$  that takes the time series as input and outputs a prediction of the label. The performance of the predictor is measured in terms of the risk  $R^d(f) = \mathbb{E}^d(\ell(f(\mathbf{X}), Y))$ . We formalize the OOD generalization problem as Problem 3.1.

##### 3.2.2 Multiple prediction tasks

Contrasting to single prediction tasks, data samples in multiple prediction tasks have multiple labels per time series:  $(\mathbf{X}, \mathbf{Y}) = (X_t, Y_p)_{t \in S_t}^{p \in S_p}$ , where  $S_t$  is the set of time steps in the time series,  $S_p \subseteq S_t$  is the set of prediction times,  $\mathbf{X}$  is the input time series observation of length  $|S_t|$  and  $\mathbf{Y}$  are the  $|S_p|$  labels. The data from domain  $d$ :  $D^d$  follows the distribution  $\mathbb{P}^d$ . We define a predictor  $f$  that takes as input the time series and outputs predictions of the labels at the prescribed prediction times. The performance of the predictor  $f$  is measured in terms of the risk  $R^d(f) = \mathbb{E}^d(\ell(f(\mathbf{X}), \mathbf{Y}))$ . We formalize the OOD generalization problem as Problem 3.1.

<sup>1</sup>In truth, the invariant features might be a transformation of the input features [85, 52]

As a stark contrast from single prediction tasks, the distribution of data  $\mathbb{P}^d$  in multiple predictions tasks can shift across data sources (e.g., images of lymph nodes from different hospitals [51]), across time (e.g., city electricity consumption across time of day) or across both source and time. We introduce these concepts with a concrete real-world example. Consider a multiple prediction regression task in finance trying to predict the next value of stock prices.

**Example 3.2** (Source-domains). A new stock market sector is to open comprising previously unseen stocks. We wish to learn a model that will predict the stock prices of this new sector. *How can we create a predictor from available training sectors (e.g., health care, energy, telecom, and others) that generalize to the unseen sector?* We can group stocks from the same sectors such that our training dataset becomes  $D^{\text{train}} = \{D^{\text{Health}}, D^{\text{Energy}}, D^{\text{Telecom}}, \dots\}$ . Solving Problem 3.1 for this dataset would lead to a predictor that generalizes to unseen market sectors as it has learned a stable solution between sources. We call this way to define domains as *Source-domains*, as time series are taken from different sources and follow different data distributions  $\mathbb{P}^d(\mathbf{X}, \mathbf{Y})$ . Domains of standard static tasks and single prediction tasks also fall into this definition of Source-domain.

**Example 3.3** (Time-domains). We wish to learn a model that will predict future stock prices. *How can we create a predictor that will generalize to the future?* We can define time intervals within data samples that we consider as different domains. For example, we can define our intervals as years and quarters  $D^{\text{train}} = \{\dots, D^{2020Q4}, D^{2021Q1}, D^{2021Q2}, D^{2021Q3}, D^{2021Q4}\}$ . This way, it becomes possible for algorithms to leverage past circumstances to find a predictor that minimizes the risk under new circumstances. Solving Problem 3.1 for this dataset would lead to a predictor that generalizes to the future as it has learned a stable solution for any future time interval. We call this way of defining domains *Time-domains*, as the time series distribution changes through time  $\mathbb{P}^d(X_t, Y_p)_{t \in S_t^d}^{p \in S_p^d}$ , where  $S_t^d$  and  $S_p^d$  are the sets of time steps and prediction times in the interval of the Time-domain  $d$  respectively.

**Remark on Time-domains** Distributional shift through time can naturally occur in any data modality [70, 117, 57, 123, 31], where the time at which the data was gathered can introduce biases, e.g., pictures gathered during summer and winter. However, intersample temporal distributional shifts can be studied under the formulation of Source-domains, where we consider different time intervals as different sources, e.g., pictures can be grouped into seasonal domains. *So when do we use the Time-domain formulation?* We use Time-domains under intrasample temporal distributional shifts, where samples cannot be split into multiple smaller sequences to consider as different sources.

Both Source-domains and Time-domains are visually depicted in Figure 2. From the raw time series samples, one can create domains by grouping subsets of time series samples, creating Source-domains, or by grouping a subset of time points, creating Time-domains.

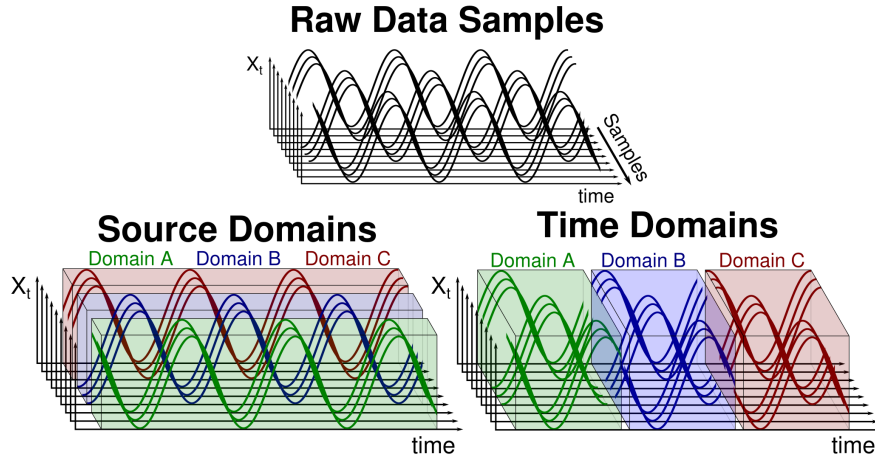


Figure 2: Visualization of the source and Time-domain definitions

## 4 Synthetic challenge datasets

We start studying the setting of OOD generalization in time series in a principled way with synthetic datasets. We propose two datasets that highlight the new challenges the time series setting brings to OOD generalization.

#### 4.1 Spurious-Fourier: Spurious features encoded in the frequency domain

Recall the cow or camel classification problem from Section 1, where a deep learning model trained to distinguish cows from camels learns to rely on the background properties (e.g., grass or sand) instead of the animal characteristic features (e.g., color and shape) to make a prediction. Arjovsky et al. [5] proposed Colored MNIST (CMNIST) to recreate the cow or camel classification problem into a simple benchmark in the image domain. In the Spurious-Fourier dataset, we adapt this same problem in the time series setting.

We create a dataset composed of one-dimensional signals, where the task is to perform binary classification based on the frequency characteristics. Signals are constructed from Fourier spectrums with one low-frequency peak ( $L$ ) and one high-frequency peak ( $H$ ). The low-frequency peak is one of the two possible frequencies ( $L_A$  or  $L_B$ ), and the high-frequency peak is also one of two possible frequencies ( $H_A$  or  $H_B$ ), see Figure 3. Domains  $D^d|_{d \in \{10\%, 80\%, 90\%\}}$  contain signal-label pairs, where the label is a noisy function of the low- and high-frequencies such that low-frequency peaks bear a varying correlation of  $d$  with the label and high-frequency peaks bear an invariant correlation of 75% with the label<sup>2</sup>.

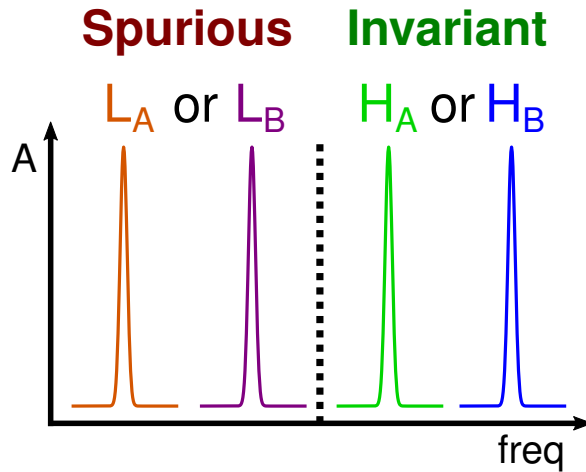


Figure 3: Fourier spectrum construction in the Spurious-Fourier dataset. Signals have one low-frequency peak ( $L$ ) and one high-frequency peak ( $H$ ). The low-frequency peak is one of two possible frequencies ( $L_A$  or  $L_B$ ), and the high-frequency peak is also one of two possible frequencies ( $H_A$  or  $H_B$ ). Signals are constructed from the Fourier spectrum with an inverse Fourier transform.

With the training dataset  $D^{\text{train}} = \{D^{80\%}, D^{90\%}\}$ , the low-frequency peaks are a stronger predictor of the label (85%) than the high-frequency peaks (75%). Therefore, minimizing the empirical risk on this dataset  $D$  will lead to a predictor that relies on the low-frequency peaks as they can achieve the lowest risk. However, the low-frequency peaks are undesirable as they are spuriously correlated and will not generalize OOD. Instead, we want to find a predictor that relies on the invariantly correlated high-frequency peaks.

**On “know it when you see it” features** In the cow or camel classification problem, having a dataset of images makes it possible to identify that some features are spuriously correlated on a “know it when you see it” basis [118], i.e., identifying that the green background and the beige background are spuriously correlated with the label. Once a spurious attribute is found in the data, it is then possible to account for it with existing distributionally robust optimization algorithms [71, 89]. However, this changes in the time series setting, as humans are not fundamentally good at extracting frequency information from the Time-domain. As a result, the discovery of spurious attributes becomes a difficult task, and without knowing the spurious attributes, we cannot account for them. We illustrate the challenge of extracting frequency information for humans in Figure 4. This problem further highlights why the time series setting is challenging under distributional shifts.

Appendix A.1 provides more information about the dataset.

<sup>2</sup>The label generation process is similar to the CMNIST dataset [5]. Appendix A.1 give more details about the creation of the Spurious-Fourier dataset.

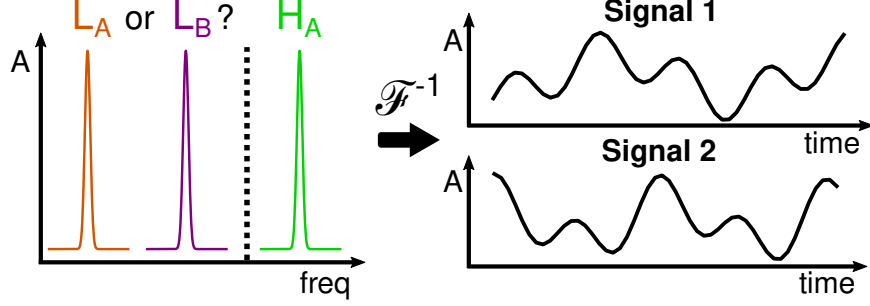


Figure 4: Visualization of the challenging task of extracting frequency information in time series as humans. Signals 1 and 2 are constructed by adding a low-frequency (either  $L_A$  or  $L_B$ ) sine wave to the high-frequency  $H_A$  sine wave. One of them has a low-frequency of  $L_A$ , while the other have the low-frequency  $L_B$ . We invite the reader to try and find which signal has the  $L_A$  frequency and which has the  $L_B$  frequency.

#### 4.2 Temporal Colored MNIST: A study of domain definitions in sequential data

In light of the previously mentioned cow or camel classification problem, Arjovsky et al. [5] proposed the CMNIST dataset as a synthetic investigation of this problem. We propose an extension of this widely used dataset to time series, where we explore new domain formulations in multiple prediction (Section 3.2.2) tasks.

In Temporal Colored MNIST (TCMNIST), we create a binary classification task of video frames. Videos are sequences of four MNIST digits where the goal is to predict whether the sum of the current and previous digits in the sequence is odd or even, see Figure 5. Prediction is made for all frames except for the first one. We use this one task definition to investigate both domain definition paradigms presented in Section 3.2: Source-domains (Example 3.2) and Time-domains (Example 3.3).

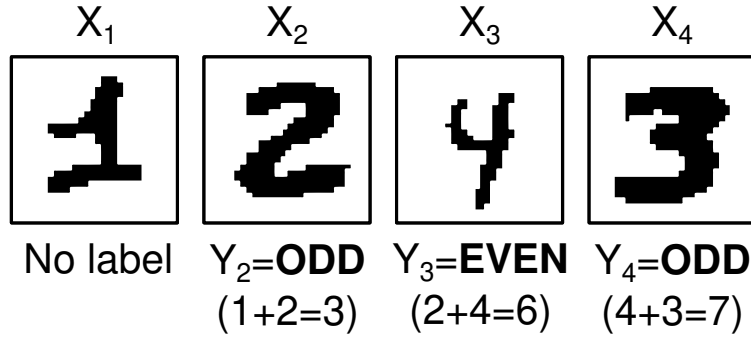


Figure 5: Task of both the TCMNIST datasets. Videos are sequences of four MNIST digits where the goal is to predict whether the sum of the current and previous digits in the sequence is odd or even.

##### 4.2.1 TCMNIST-Source

Domains  $D^d|_{d \in \{10\%, 80\%, 90\%\}}$  contain videos where each frame depicts a digit colored either red or green (except for the first digit which is yellow). The label is a noisy function of the digit and color, such that the color bears a varying correlation of  $d$  with the label of the frame, and the digit information bears an invariant correlation of 75% with the label of the frame. The color correlation varies between sequences belonging to different domains but is constant among the video frames. The domain definition is visually depicted in Figure 6.

Just like CMNIST, the color is spuriously correlated with the label, while the sum of digits is invariantly correlated with the label. We want to find a predictor that relies on the depicted digit to predict the label.

Appendix A.2 provides more information about this dataset.

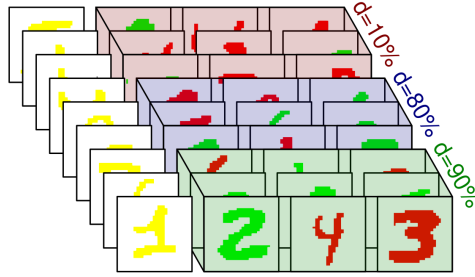


Figure 6: Domain definition for the Temporal Colored MNIST with Source-domains (TCMNIST-Source) dataset. Videos are created from the domain definition they are sampled from, i.e., the spurious correlation value is constant throughout the frames of a video, but it changes between domains.

#### 4.2.2 TCMNIST-Time

Video frames are grouped according to their order in the sequence and they form the domains  $D^d|_{d \in \{90\%, 80\%, 10\%\}}$ . A single video sequence consists of video frames from multiple domains, where the domains always follow the same sequence: [90%, 80%, 10%]. The first frame does not have a domain, because it does not have a label. Similarly to the Source-domains, the label is a noisy function of the digit and color, such that the color bears a varying correlation of  $d$  with the label of the frame, and the sum of digits bears an invariant correlation of 75% with the label of the frame. The color correlation varies between the video frames, but is constant between all sequences in the dataset. The domain definition and time series structure are visually depicted in Figure 7.

Appendix A.2 provides more information about this dataset.

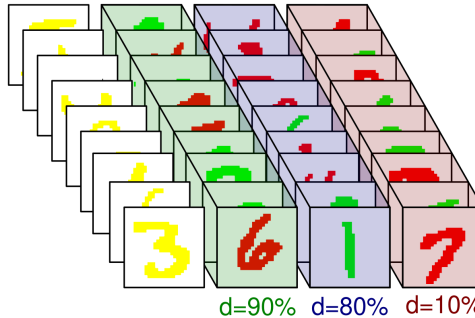


Figure 7: Domain definition for the Temporal Colored MNIST with Time-domains (TCMNIST-Time) dataset. Videos are created by sequentially sampling frames from different domains, i.e. the spurious correlation value varies throughout the frames of a video, but the sequence of correlation value is always the same between videos.

## 5 Real-world datasets

The WOODS datasets are challenging with respect to their distributional shifts. Significant distributional shifts that lead to a large generalization gap between training and testing help us differentiate between algorithms that provide meaningful improvement and algorithms that provide marginal improvement.

The WOODS datasets also target unresolved problems in their respective fields of study. Thus, this set of benchmarks not only serves to evaluate the performance of OOD generalization algorithms but also serves the field of study from which they stem. Progress on any of our datasets would be mutually beneficial for both the OOD generalization field and the associated application research field.

The WOODS datasets were gathered from various open-source repositories [28, 23, 45]. The raw datasets were preprocessed according to standards in their respective fields.

Appendix A provides all preprocessing steps along with the licenses for each of the datasets.



### 5.1 CAP: Sleep classification across different machines

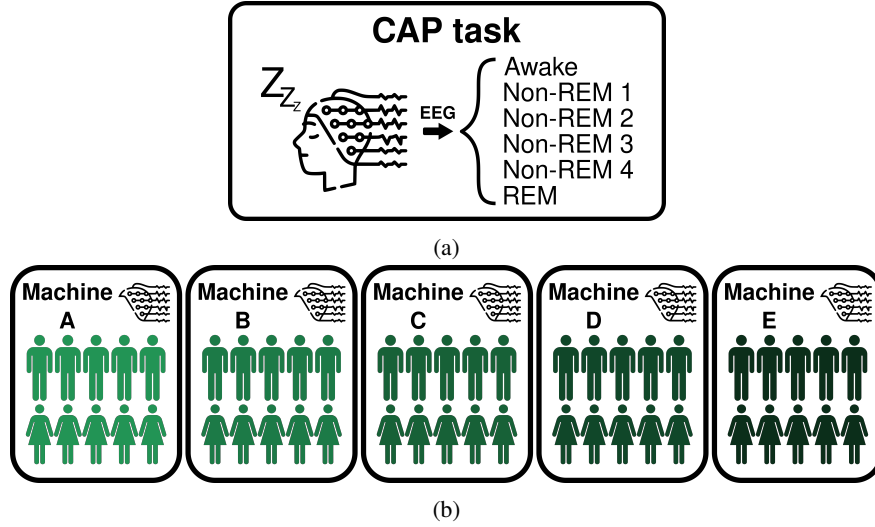


Figure 8: Description of the CAP dataset, where (a) the task is to perform sleep stage classification from electroencephalographic (EEG) measurements, and (b) the domains are different machines.

A recurrent problem in computational medicine is that models trained on data from a given recording machine will not generalize to data coming from another machine, even when both machines are from a similar constructor. Failure to generalize to unseen machines can cause critical issues for clinical practice because a false sense of confidence in a model could lead to a false diagnosis. Furthermore, even when following the exact same data gathering procedures, a change in the recording machinery can lead to catastrophic distributional shifts. We study these machinery-induced distribution shifts with the CAP dataset (Figure 8).

We consider the sleep stage classification task from electroencephalographic (EEG) measurements. The labels are six sleep stages (i.e., Awake, Non-REM 1-2-3-4, and REM) labeled by experts in the field. The data comes from five different machines, which act as our five Source-domains. The goal is to generalize to unseen machines. As a whole, the dataset is composed of 40390 recordings of 30 seconds each from 19 EEG channels gathered on 41 participants.

Appendix A.3 provides more information about the dataset.

### 5.2 SEDFx: Sleep Classification across age groups

In clinical settings, we train a model on the data gathered from a limited number of patients and hope this model will generalize to unseen patients in the future [78]. However, this generalization between observed patients in the training dataset and new patients at the test time is not guaranteed. Distributional shifts caused by shifts in patient demographics (e.g., age, gender, and ethnicity) can cause the model to fail. We study these patient demographic shifts with the SEDFx dataset (Figure 9).

We consider the sleep classification task from EEG measurements. The labels are six sleep stages (Awake, Non-REM 1-2-3-4, and REM) labeled by experts in the field. The data comes from five age groups, which act as our Source-domains. The goal is to generalize to an unseen age demographic. As a whole, the dataset is composed of 238712 recordings of 30 seconds each from four EEG channels gathered on 100 participants.

Appendix A.4 provides more information about the dataset.

### 5.3 PCL: Motor imagery classification across data-gathering procedures

Aside from changes in the recording device and shifts in patient demographics, human intervention in the data gathering process is another contributing factor to the distributional shift that can lead to failure of clinical models. Specifically, a small change in the data-gathering procedures can cause procedural shifts that cause models to fail to generalize to other data gathering procedures. One known instance of this failure mode is the Camelyon17 [51] dataset, where models fail to generalize to other hospitals because of differences in the staining procedure of lymph node slices. This challenge is especially prevalent in temporal medical data (e.g., EEG, MEG, and others) because recording devices are complex

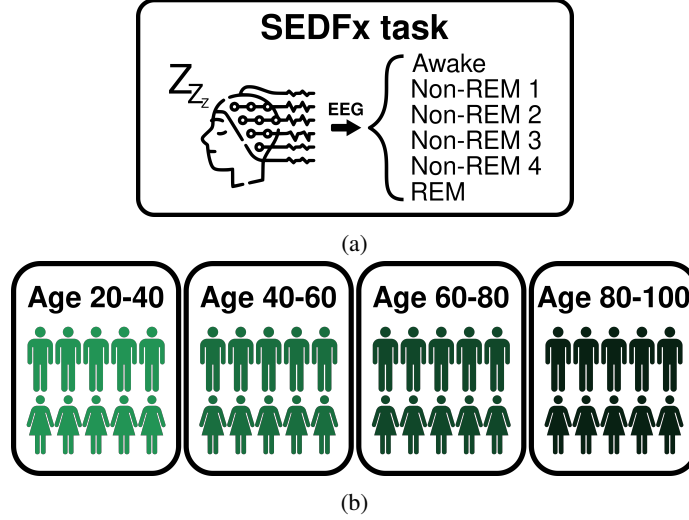


Figure 9: Description of the SEDFx dataset, where (a) the task is to perform sleep stage classification from electroencephalographic (EEG) measurements, and (b) the domains are different age demographics.

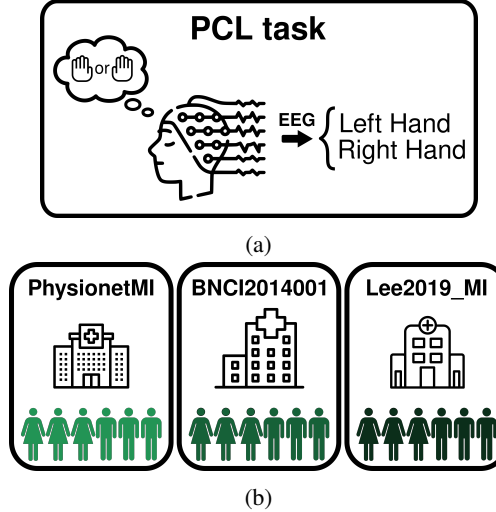


Figure 10: Description of the PCL dataset, where (a) the task is to perform motor imagery classification from electroencephalographic (EEG) measurements, and (b) the domains are different hospitals.

tools greatly affected by nonlinear effects and modulations. These effects are often caused by context and preparations made before the recording [24]. We study these procedural shifts on the PCL dataset (Figure 10).

We consider the motor imagery task from electroencephalographic (EEG) measurements. The labels are two imagined movements (left hand and right hand). The dataset comes from three different hospitals performing the same task under different data gathering procedures and conditions. They act as our Source-domains. The goal is to generalize to unseen data gathering processes. As a whole, the dataset is composed of 22598 recordings of three seconds each from 48 EEG channels gathered with 215 participants.

Appendix A.5 provides more information about the dataset.

#### 5.4 LSA64: Sign language video classification across speakers

Communication is an idiosyncratic way to convey information through different media: text, speech, body language, and many others. However, some media are more distinctive and challenging than others. For example, text communication has less interindividual variability than body language or speech. If deep learning systems hope to interact with

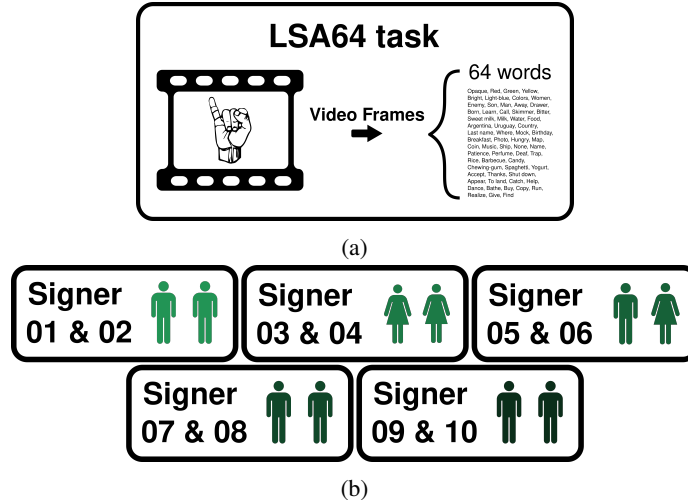


Figure 11: Description of the LSA64 dataset, where (a) the task is to perform signed words classification from videos, and (b) the domains are different signers.

humans effectively, models need to generalize to previously unseen mannerisms, accents, and other subtle variations in communication that significantly impact the meaning of the message conveyed. We study the ability of models to recognize information coming from unseen individuals in the LSA64 dataset (Figure 11).

We consider the video classification of signed words in Argentinian Sign Language. The labels are a dictionary of 64 words. The dataset consists of ten different signers making multiple repetitions of all 64 words. From that, we create five Source-domains consisting of two speakers each. The goal is to generalize to unseen signers. As a whole, the dataset is composed of 3200 videos of two and a half seconds each at a resolution of (3,224,224).

Appendix A.6 provides more information about the dataset.

## 5.5 HHAR: Human activity recognition across smart devices

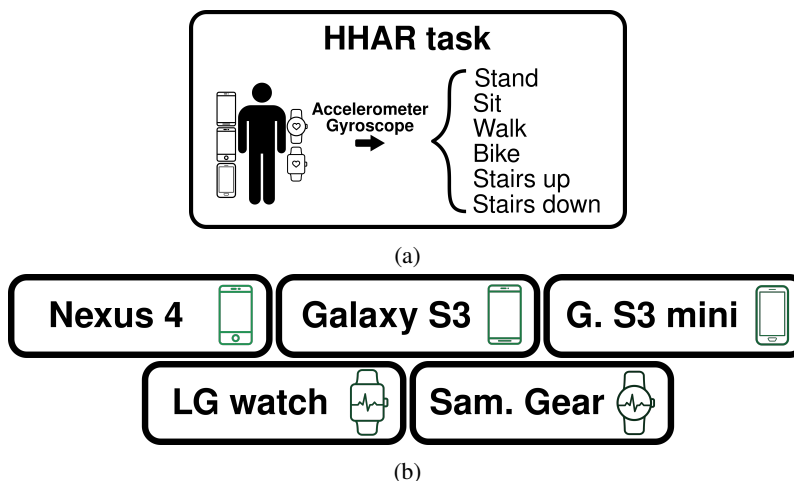


Figure 12: Description of the HHAR dataset, where (a) the task is to perform human activity classification from smart devices sensor data, and (b) the domains are different smart devices.

Invariant features needed to make predictions in time series are highly convoluted in time with other uninformative features. Because of this, it is a difficult task to extract invariant temporal features from data. We study the ability of models to ignore uninformative information from complex signals with the HHAR dataset (Figure 12).

We consider the human activity classification task from smart devices (smartphones and smartwatches) sensor data. Sensor data consists of three-axis accelerometer measurements and three-axis gyroscope measurements. The labels are six activities (Stand, Sit, Walk, Bike, Stairs up, and Stairs Down). The data originates from five different devices, which act as our Source-domains. The goal is to find the invariant sensory features across phones and watches. Because watches and cellphones are not worn in the same place on the body, one might have extra oscillations that the model should disregard. As a whole, the dataset is composed of 13674 recordings of five seconds each from six sensor channels.

Appendix A.7 provides more information about the dataset.

## 6 Measuring the impact of distributional shifts

The WOODS datasets are chosen for their significant distribution shifts that cause drops in the performance of models evaluated on unseen domains. We use the *generalization gap* to empirically measure the impact of the distribution shifts on the performance of models. It measures the drop in performance between data drawn In-Distribution (ID) and Out-of-Distribution (OOD), where the former is independent and identically distributed (i.i.d.) to the training distribution and the later is not i.i.d. but has some restriction with respect to the training distribution as discussed in Section 3.1. However, the generalization gap can be a misleading measure as it does not intrinsically indicate attainable performance gains. Appendix B provides such an example. In this work, we try to provide a good measure of the achievable performance gain for a dataset, i.e., an upper bound to the achievable performance on unseen domains.

How do we measure this gap? Given a set of training domains  $D^{\text{train}}$  and a test domain  $D^{\text{test}}$ , we first measure the *OOD performance* by training a model on the training domains  $D^{\text{train}}$  with ERM and measure the performance of this model on the test domain  $D^{\text{test}}$ . Second, we measure the *ID performance* with the mixed-to-test measure [51], where we train a model on all domains  $D = \cup_{d \in \{\text{train}, \text{test}\}} D^d$  and evaluate the model on the test domain  $D^{\text{test}}$ . The generalization gap for that test domain is then defined as the difference between the ID and OOD performance. That process can then be repeated for all domains in the dataset for a cross-validation style measure of the gap.

Although the ID performance can be obtained in multiple ways [51], we choose the mixed-to-test definition because it best fits our goal of finding an upper bound of performance. Appendix B discusses other approaches to measuring ID performance and why we use the mixed-to-test measure.

## 7 Adaptation of baseline algorithms

Many algorithms were proposed to address the failure of machine learning models under distributional shifts. However, they were initially formulated for the image domain and require adaptation to be used with time series. This section describes the baseline algorithms we use and how we adapted them to the time series settings.

### Baselines algorithms

- Empirical Risk Minimization (**ERM**, Vapnik [110]) minimizes the average empirical risk across domains.
- Invariant Risk Minimization (**IRM**, Arjovsky et al. [5]) performs a constrained ERM such that the optimal classifier of representations is the same across the domains.
- Variance Risk Extrapolation (**VREx**, Krueger et al. [54]) performs ERM while minimizing the variance of risk across domains.
- Spectral Decoupling (**SD**, Pezeshki et al. [77]) performs ERM while minimizing the L2 norm of the logits.
- Information Bottleneck Empirical Risk Minimization (**IB-ERM**, Ahuja et al. [3]) performs ERM while minimizing the variance of the representations.

All baseline algorithms in this work are penalized versions of ERM that take the form of

$$\mathcal{L}(f) = \frac{1}{N_d} \sum_{d \in \mathcal{E}_{\text{train}}} R^d(f) + \lambda \cdot P(f), \quad (1)$$

where  $N_d$  is the number of training domains, and  $P(f)$  is the penalized value, e.g., VREx [54] penalizes the variance of the empirical risk between domains such that  $P(f) = \text{Var}(R^d(f))$ .

## 7.1 Single prediction tasks

A single prediction task (Section 3.2.1) means predicting one label at the end of a time series. This setting is directly analogous to image classification tasks where we predict one label per image. Therefore, the adaptation is trivial as we can use the penalized form of ERM at Equation (1) and backpropagate through time [30].

## 7.2 Multiple predictions tasks

A multiple prediction task (Section 3.2.2) means predicting multiple labels in a time series. Therefore, we need to adapt the definition of the empirical risk  $R^d(f)$  and the penalized value  $P(f)$  in Equation (1) to account for the multiple predictions.

**Empirical risk** As is custom in time series tasks, we average the empirical risk across predictions in the time series. However, across what we average the risk across will vary with whether we define domains as Source-domains (Example 3.2) or Time-domains (Example 3.3). For Source-domains, we average the empirical risk of a domain across all predictions in the time series

$$R^d(f) = \frac{1}{|S_p|} \sum_{t \in S_p} R_t^d(f), \quad (2)$$

where  $S_p$  is the set of all prediction times in the time series. For Time-domains, we average the empirical risk across the interval of the domain

$$R^d(f) = \frac{1}{|S_p^d|} \sum_{t \in S_p^d} R_t^d(f), \quad (3)$$

where  $S_p^d$  is the set of prediction times made in the interval of domain  $d$ .

**Penalized value** Generally, the adaptation of OOD generalization algorithms to time series will need to be made on a case-by-case basis as they can take many different forms. However, our baselines can be grouped into two groups that function in similar ways and therefore will be adapted in similar ways.

The first group is algorithms that penalize a function of the empirical risk (i.e., IRM and VREx). For those, we use the averaged risk defined in Equation (2) for Source-domains, and Equation (3) for Time-domains. As an example, the VREx penalty remains  $P(f) = \text{Var}(R^d(f))$ , but the definition of  $R^d(f)$  changes with the domain definition.

The second group is algorithms that penalize representations of the model (i.e., SD and IB-ERM). For those, we average the penalized metric across the prediction times in the same way we average the empirical risk. For example, the SD penalty becomes  $P(f) = \frac{1}{|S_p|} \sum_{t \in S_p} \|f(X_{1:t})\|^2$  for Source-domains, and  $P(f) = \frac{1}{|S_p^d|} \sum_{t \in S_p^d} \|f(X_{1:t})\|^2$  for Time-domains.

## 8 Evaluation framework

Along with our set of time series benchmarks, we also provide a framework for a fair and systematic evaluation of OOD performance for the current and future algorithms. We follow the DomainBed [29] testbed workflow for hyperparameter tuning and model selection.

Appendix D provides more information on the framework along with implementation details. Appendix E provides more information on the hyperparameter search spaces used for our baselines.

### 8.1 Model Selection

We create many models during the training process due to repeated training across different hyperparameters, weight initialization, dataset splits, and training steps. Then, we have to find a model among those created that, we think, will generalize to the test domains. However, a fundamental restriction in OOD generalization is that we do not have access to the test domains during training. As a result, the challenge of OOD generalization is not only to create models that generalize to the test domains but also to select the right models without having access to the test domains. To address this, many model selection criteria were proposed [29, 122, 51]. For example, Gulrajani and Lopez-Paz [29] proposed *Train-domain validation*.

**Train-domain validation** We split the training domains into training and validation sets. The training split of the training domain is used to train the model, while the validation split is used to evaluate the model on unseen data drawn i.i.d. to the training split. We choose the model that gets the best average validation performance across training domains. We report the performance of the chosen model on the testing domains.

However, tackling both problems of creating and finding invariant models at the same time might be a very difficult research endeavor. Instead, we can first start by narrowing the scope and only focus on creating invariant models. For this purpose, we relax the fundamental restriction and allow the queries of the test domain to obtain some signal on the absolute performance of an algorithm. Although querying the test domain can never be considered a valid model selection strategy in practical scenarios, the results can be very insightful when evaluating the behavior of an algorithm. Gulrajani and Lopez-Paz [29] formulated *Test-domain validation* that queries the test domains to perform model selection.

**Test-domain validation** We split the test domains into testing and validation sets. Models are trained for a fixed number of training steps on the training domains. We choose the model with the best performance on the validation set of the test domains. We only consider the final checkpoint of the model after a fixed number of steps, effectively disallowing early stopping. We report the performance of the chosen model on the testing set of test domains.

Test-domain validation has proven to be a very useful measure of performance for algorithms on synthetic datasets driven primarily by correlation shift [122], e.g., CMNIST. In such datasets, simple spurious features highly correlated with the label create shortcuts in the data that model leverage to minimize the empirical risk quickly (e.g., cow or camel classification problem). As a result, these shortcuts lead to very high training domain performance and very low test domain performance early in training. Consequently, any model selection criteria that rely on performance on data drawn i.i.d. to the training distribution is a poor way to investigate the performance of an algorithm because there is a bias of model selection towards early training correlation. Thus, by disallowing early stopping, we obtain an insightful measure to investigate the absolute performance of an algorithm.

On the other hand, Test-domain validation is ill-equipped to provide meaningful measures of performance with other kinds of datasets. For example, Test-domain validation is not an insightful measure of performance when dealing with real-world datasets. The reason is that we often do not know beforehand the number of training steps required for a given set of hyperparameters such that a model will finish the learning of the task. Therefore, we train models past the point of overfitting and pick the model with the highest validation performance. This renders the last checkpoint in training suboptimal for generalization performance, both ID and OOD, and leads to an uninformative measure of the generalization performance.

We introduce a more pragmatic model selection method that queries the test domain for real-world datasets to resolve this problem: *Oracle train-domain validation*.

**Oracle train-domain validation** We split the training domains into training and ID validation splits. We also split the test domains into testing and OOD validation splits. For every model training run, we choose the early stopped model that performs best on the ID validation split. We then choose the chosen early stopped model that performs the best in the OOD validation split. Notice that this model selection method has the same number of queries of the test domain as the test-domain validation, i.e., one query per training run.

In light of the discussion of this section, we use two different sets of model selection methods for the two different types of datasets in WOODS: Synthetic challenge and real-world datasets. We use **train-domain validation** and **test-domain validation** for our synthetic challenge datasets driven by correlation shift. We use **train-domain validation** and **oracle train-domain validation** for our real-world datasets which are likely driven by other kinds of shifts.

## 8.2 Model architecture choices

Time series tasks require a specific architecture depending on the task and data modality [115, 42, 109]. For example, state-of-the-art architectures for processing EEG signals are considerably different from state-of-the-art architectures for processing video. In our work, we provide specific architectures tailored to the dataset modality and tasks. However, we do not choose architectures based on the state-of-the-art at the time of writing. Instead, we chose architectures that are common within the field associated with the data modality and provide good performance.

Appendix A provides more information on architecture choices for every dataset.

## 9 Results

Through extensive experimentation on our eight datasets, we draw four major conclusions:

**WOODS datasets have a significant generalization gap** Table 1 summarizes the generalization gap for all WOODS datasets, along with the ID and OOD performance. The ID performance is computed by training ERM on all available domains of a dataset, choosing the best model for train domain validation, and report the average performance over all domains<sup>3</sup>. The OOD performance is computed by taking the cross-validated measure of the generalization performance of ERM with train-domain validation (see Table 3 and 4). As discussed in Section 6, generalization gaps are computed to be an upper bound of the attainable performance on the test domains. This is positively indicative that there is an improvement to be made over ERM.

Dataset	Performance		Gap
	ID	OOD	
Spurious-Fourier	74.45 $\pm$ 0.1	9.75 $\pm$ 0.2	64.70
TCMNIST			
Source Dom.	68.36 $\pm$ 0.1	10.15 $\pm$ 0.1	58.21
Time Dom.	89.36 $\pm$ 0.0	10.04 $\pm$ 0.0	79.32
CAP	75.12 $\pm$ 0.7	62.63 $\pm$ 0.4	12.49
SEDFx	72.48 $\pm$ 0.4	69.28 $\pm$ 0.9	3.20
PCL	73.64 $\pm$ 0.2	64.71 $\pm$ 0.3	8.93
HHAR	93.35 $\pm$ 0.4	84.28 $\pm$ 0.4	9.07
LSA64	86.56 $\pm$ 1.0	49.48 $\pm$ 1.2	37.08

Table 1: Classification accuracy drop of ERM between ID generalization and OOD generalization. The ID performance is computed by training ERM on all available domains of a dataset, choosing the best model with train-domain validation and report the average performance over all domains (except for the synthetic challenge datasets we only evaluate on the target test domain). The OOD performance is computed by taking the cross-validated measure of the generalization performance of ERM with train-domain validation (see Table 3 and 4)

**Models can learn time specific spurious correlations** Models can learn multiple spurious correlations for different time steps in time series. We see this in Table 2, obtained by training ERM on all domains of the TCMNIST-Time dataset, i.e., the full videos. We see that the models can get performance above the invariant solution correlation (75%) on all domains of the dataset. This is possible because models are implicitly given the domain definition by virtue of the data structure. This allows them to learn multiple spurious correlations in a sequence by knowing the time steps of the prediction. This behavior is impossible in the Source-domain setting because models are agnostic to the domains. To summarize, these new ways for models to latch to spurious correlations highlights the challenge that time series bring to the field of OOD generalization.

80%	90%	10%
80.98 $\pm$ 0.02	91.20 $\pm$ 0.00	89.97 $\pm$ 0.00

Table 2: ID results for the TCMNIST-Time dataset

**A familiar story for IRM and VREx on WOODS’ synthetic challenge datasets** Table 3 summarizes the baseline results on our synthetic challenge datasets. We observe that IRM and VREx are both able to create models that generalize well OOD during training on the synthetic challenge datasets, as shown by good performance on Test-domain validation. However, none are able to find those invariant models with train-domain validation. Additionally, IRM seems to be better behaved when dealing with Time-domains.

**Marginal improvement over ERM on WOODS’ real-world datasets** Table 4 summarizes the baseline results on our real-world datasets likely driven by covariate shifts. We observe a marginal improvement over ERM for SD and IB-ERM.

<sup>3</sup>for the synthetic challenge datasets we only evaluate on the target test domain

Train-domain validation				
Objective	Spurious-Fourier	TCMNIST		Average
		Source-domains	Time-domains	
ERM	$9.75 \pm 0.23$	$10.15 \pm 0.13$	$10.04 \pm 0.00$	9.98
IRM	$9.35 \pm 0.09$	$9.98 \pm 0.00$	$10.04 \pm 0.00$	9.79
VREx	$9.77 \pm 0.20$	$10.00 \pm 0.01$	$10.05 \pm 0.00$	9.94
IB-ERM	$10.08 \pm 0.37$	$10.00 \pm 0.00$	$10.05 \pm 0.01$	10.05
SD	$10.28 \pm 0.16$	$10.01 \pm 0.01$	$10.05 \pm 0.00$	10.11

Test-domain validation				
Objective	Spurious-Fourier	TCMNIST		Average
		Source-domains	Time-domains	
ERM	$9.30 \pm 0.07$	$27.37 \pm 2.09$	$25.78 \pm 4.70$	20.82
IRM	$57.68 \pm 0.84$	$52.11 \pm 1.24$	$53.66 \pm 2.14$	54.48
VREx	$65.39 \pm 4.84$	$50.39 \pm 0.34$	$36.91 \pm 10.98$	50.90
IB-ERM	$9.28 \pm 0.05$	$20.81 \pm 1.14$	$24.71 \pm 1.58$	18.27
SD	$9.25 \pm 0.03$	$24.12 \pm 3.33$	$22.06 \pm 3.21$	18.48

Table 3: Summary of baseline performance on the synthetic challenge datasets. We report only the performance on the intended test domain, i.e., the 10% domain, for all our synthetic challenge datasets to avoid diluting the result with easier training domain configurations.

Train-domain validation						
Objective	CAP	SEDFx	PCL	HHAR	LSA64	Average
ERM	$62.63 \pm 0.37$	$69.28 \pm 0.86$	$64.71 \pm 0.27$	$84.28 \pm 0.37$	$49.48 \pm 1.20$	66.08
IRM	$58.40 \pm 1.00$	$62.53 \pm 0.53$	$63.71 \pm 0.86$	$81.08 \pm 0.44$	$45.03 \pm 1.60$	62.15
VREx	$57.47 \pm 0.88$	$57.97 \pm 0.54$	$63.48 \pm 0.79$	$81.58 \pm 0.52$	$46.11 \pm 2.88$	61.32
IB-ERM	$62.80 \pm 0.62$	$69.48 \pm 0.47$	$64.44 \pm 0.32$	$83.53 \pm 0.74$	$57.28 \pm 1.88$	67.51
SD	$60.76 \pm 0.92$	$69.84 \pm 0.49$	$64.40 \pm 0.24$	$85.63 \pm 0.15$	$50.74 \pm 1.72$	66.27

Oracle train-domain validation						
Objective	CAP	SEDFx	PCL	HHAR	LSA64	Average
ERM	$64.00 \pm 0.52$	$70.61 \pm 0.47$	$65.19 \pm 0.17$	$85.01 \pm 0.19$	$56.82 \pm 0.52$	68.33
IRM	$59.84 \pm 0.91$	$63.23 \pm 0.32$	$63.95 \pm 0.82$	$81.49 \pm 0.28$	$46.48 \pm 1.61$	63.00
VREx	$58.22 \pm 0.47$	$59.29 \pm 0.31$	$64.03 \pm 0.59$	$82.49 \pm 0.29$	$52.32 \pm 0.56$	63.27
IB-ERM	$63.98 \pm 0.52$	$70.64 \pm 0.43$	$65.04 \pm 0.31$	$85.52 \pm 0.22$	$59.78 \pm 1.03$	68.99
SD	$63.20 \pm 0.42$	$70.60 \pm 0.36$	$65.34 \pm 0.12$	$86.30 \pm 0.16$	$58.62 \pm 1.01$	68.81

Table 4: Summary of baseline performance on real-world datasets

## 10 Conclusion, limitation & future work

This work introduced WOODS: a set of eight open-source benchmarks for OOD generalization in time series tasks and its evaluation framework. We formulated the Time-domain setting for dealing with intrasample temporal distribution shifts. Next, we proposed a new model selection method for a more pragmatic use in real-world datasets. Finally, we adapted standard OOD algorithms to the time series setting and provided their performance on our benchmarks as baselines for future work.

**Limitations and future work.** Even though we formulated the theory around multiple prediction tasks and Time-domains in OOD generalization, we do not currently have real-world datasets for those settings. We hope for WOODS to continue building towards a complete set of benchmarks with datasets covering those missing settings and other data modalities not currently studied in WOODS.



## 11 Acknowledgments

Kartik Ahuja acknowledges the support provided by IVADO postdoctoral fellowship funding program. Guillaume Dumas acknowledges the support from the Institute for Data Valorization (IVADO), Montréal and the Fonds de recherche du Québec (FRQ). Irina Rish acknowledges the support from Canada CIFAR AI Chair Program and from the Canada Excellence Research Chairs program.

We thank Vikram Voleti for code review and general help with the WOODS code base. We thank Nadhir-Vincent Hassen and Remus Mocanu for general help with the WOODS code base. We also thank Parviz Haggi-Mani for insightful discussions pertaining to the formulation of domains in time series.

## References

- [1] Kartik Ahuja, Karthikeyan Shanmugam, Kush Varshney, and Amit Dhurandhar. Invariant risk minimization games. In *International Conference on Machine Learning*, pages 145–155. PMLR, 2020.
- [2] Kartik Ahuja, Jun Wang, Amit Dhurandhar, Karthikeyan Shanmugam, and Kush R Varshney. Empirical or invariant risk minimization? a sample complexity perspective. *arXiv preprint arXiv:2010.16412*, 2020.
- [3] Kartik Ahuja, Ethan Caballero, Dinghuai Zhang, Jean-Christophe Gagnon-Audet, Yoshua Bengio, Ioannis Mitliagkas, and Irina Rish. Invariance principle meets information bottleneck for out-of-distribution generalization. *Advances in Neural Information Processing Systems*, 34, 2021.
- [4] Torben G Andersen, Tim Bollerslev, Peter Christoffersen, and Francis X Diebold. Volatility forecasting, 2005.
- [5] Martin Arjovsky, Léon Bottou, Ishaan Gulrajani, and David Lopez-Paz. Invariant risk minimization, 2020.
- [6] Benjamin Aubin, Agnieszka Słowik, Martin Arjovsky, Leon Bottou, and David Lopez-Paz. Linear unit-tests for invariance discovery, 2021.
- [7] Claudine Badue, Rânik Guidolini, Raphael Vivacqua Carneiro, Pedro Azevedo, Vinicius B Cardoso, Avelino Forechi, Luan Jesus, Rodrigo Berriel, Thiago M Paixao, Filipe Mutz, et al. Self-driving cars: A survey. *Expert Systems with Applications*, 165:113816, 2021.
- [8] Shaojie Bai, J Zico Kolter, and Vladlen Koltun. An empirical evaluation of generic convolutional and recurrent networks for sequence modeling. *arXiv preprint arXiv:1803.01271*, 2018.
- [9] Andrei Barbu, David Mayo, Julian Alverio, William Luo, Christopher Wang, Dan Gutfreund, Josh Tenenbaum, and Boris Katz. Objectnet: A large-scale bias-controlled dataset for pushing the limits of object recognition models. *Advances in neural information processing systems*, 32, 2019.
- [10] Loïc Barrault, Ondřej Bojar, Marta R. Costa-jussà, Christian Federmann, Mark Fishel, Yvette Graham, Barry Haddow, Matthias Huck, Philipp Koehn, Shervin Malmasi, Christof Monz, Mathias Müller, Santanu Pal, Matt Post, and Marcos Zampieri. Findings of the 2019 conference on machine translation (WMT19). In *Proceedings of the Fourth Conference on Machine Translation (Volume 2: Shared Task Papers, Day 1)*, pages 1–61, Florence, Italy, August 2019. Association for Computational Linguistics. doi: 10.18653/v1/W19-5301. URL <https://aclanthology.org/W19-5301>.
- [11] Sara Beery, Grant van Horn, and Pietro Perona. Recognition in terra incognita, 2018.
- [12] James Bergstra and Yoshua Bengio. Random search for hyper-parameter optimization. *Journal of machine learning research*, 13(2), 2012.
- [13] Joos-Hendrik Böse, Valentin Flunkert, Jan Gasthaus, Tim Januschowski, Dustin Lange, David Salinas, Sebastian Schelter, Matthias Seeger, and Yuyang Wang. Probabilistic demand forecasting at scale. *Proceedings of the VLDB Endowment*, 10(12):1694–1705, 2017.
- [14] Tom Brown, Benjamin Mann, Nick Ryder, Melanie Subbiah, Jared D Kaplan, Prafulla Dhariwal, Arvind Neelakantan, Pranav Shyam, Girish Sastry, Amanda Askell, et al. Language models are few-shot learners. *Advances in neural information processing systems*, 33:1877–1901, 2020.
- [15] César Capinha, Ana Ceia-Hasse, Andrew M Kramer, and Christiaan Meijer. Deep learning for supervised classification of temporal data in ecology. *Ecological Informatics*, 61:101252, 2021.
- [16] Daniel Cer, Mona Diab, Eneko Agirre, Inigo Lopez-Gazpio, and Lucia Specia. Semeval-2017 task 1: Semantic textual similarity-multilingual and cross-lingual focused evaluation. *arXiv preprint arXiv:1708.00055*, 2017.
- [17] Yongqiang Chen, Yonggang Zhang, Han Yang, Kaili Ma, Binghui Xie, Tongliang Liu, Bo Han, and James Cheng. Invariance principle meets out-of-distribution generalization on graphs. *arXiv preprint arXiv:2202.05441*, 2022.

- [18] Travers Ching, Daniel S Himmelstein, Brett K Beaulieu-Jones, Alexandr A Kalinin, Brian T Do, Gregory P Way, Enrico Ferrero, Paul-Michael Agapow, Michael Zietz, Michael M Hoffman, et al. Opportunities and obstacles for deep learning in biology and medicine. *Journal of The Royal Society Interface*, 15(141):20170387, 2018.
- [19] Hohyun Cho, Minkyu Ahn, Sangtae Ahn, Moonyoung Kwon, and Sung Chan Jun. Eeg datasets for motor imagery brain-computer interface. *GigaScience*, 6(7):gix034, 2017.
- [20] Sylvain Christin, Éric Hervet, and Nicolas Lecomte. Applications for deep learning in ecology. *Methods in Ecology and Evolution*, 10(10):1632–1644, 2019.
- [21] Róbert Csordás, Kazuki Irie, and Jürgen Schmidhuber. The devil is in the detail: Simple tricks improve systematic generalization of transformers. *arXiv preprint arXiv:2108.12284*, 2021.
- [22] Chirag Deb, Fan Zhang, Junjing Yang, Siew Eang Lee, and Kwok Wei Shah. A review on time series forecasting techniques for building energy consumption. *Renewable and Sustainable Energy Reviews*, 74:902–924, 2017.
- [23] Dheeru Dua and Casey Graff. UCI machine learning repository, 2017. URL <http://archive.ics.uci.edu/ml>.
- [24] Denis A Engemann, Federico Raimondo, Jean-Rémi King, Benjamin Rohaut, Gilles Louppe, Frédéric Faugeras, Jitka Annen, Helena Cassol, Olivia Gosseries, Diego Fernandez-Slezak, et al. Robust eeg-based cross-site and cross-protocol classification of states of consciousness. *Brain*, 141(11):3179–3192, 2018.
- [25] Haoqi Fan, Tullie Murrell, Heng Wang, Kalyan Vasudev Alwala, Yanghao Li, Yilei Li, Bo Xiong, Nikhila Ravi, Meng Li, Haichuan Yang, Jitendra Malik, Ross Girshick, Matt Feiszli, Aaron Adcock, Wan-Yen Lo, and Christoph Feichtenhofer. PyTorchVideo: A deep learning library for video understanding. In *Proceedings of the 29th ACM International Conference on Multimedia*, 2021. <https://pytorchvideo.org/>.
- [26] Robert Geirhos, Jörn-Henrik Jacobsen, Claudio Michaelis, Richard Zemel, Wieland Brendel, Matthias Bethge, and Felix A. Wichmann. Shortcut learning in deep neural networks. *Nature Machine Intelligence*, 2(11):665–673, Nov 2020. ISSN 2522-5839. doi: 10.1038/s42256-020-00257-z. URL <http://dx.doi.org/10.1038/s42256-020-00257-z>.
- [27] Muhammad Ghifary, W Bastiaan Kleijn, Mengjie Zhang, and David Balduzzi. Domain generalization for object recognition with multi-task autoencoders. In *Proceedings of the IEEE international conference on computer vision*, pages 2551–2559, 2015.
- [28] A. L. Goldberger, L. A. N. Amaral, L. Glass, J. M. Hausdorff, P. Ch. Ivanov, R. G. Mark, J. E. Mietus, G. B. Moody, C.-K. Peng, and H. E. Stanley. PhysioBank, PhysioToolkit, and PhysioNet: Components of a new research resource for complex physiologic signals. *Circulation*, 101(23):e215–e220, 2000. Circulation Electronic Pages: <http://circ.ahajournals.org/content/101/23/e215.full> PMID:1085218; doi: 10.1161/01.CIR.101.23.e215.
- [29] Ishaan Gulrajani and David Lopez-Paz. In search of lost domain generalization, 2020.
- [30] Jiang Guo. Backpropagation through time. *Unpubl. ms., Harbin Institute of Technology*, 40:1–6, 2013.
- [31] Lin Lawrence Guo, Stephen R Pfohl, Jason Fries, Alistair EW Johnson, Jose Posada, Catherine Aftandilian, Nigam Shah, and Lillian Sung. Evaluation of domain generalization and adaptation on improving model robustness to temporal dataset shift in clinical medicine. *Scientific reports*, 12(1):1–10, 2022.
- [32] Ruining He and Julian McAuley. Ups and downs: Modeling the visual evolution of fashion trends with one-class collaborative filtering. In *proceedings of the 25th international conference on world wide web*, pages 507–517, 2016.
- [33] Yue He, Zheyang Shen, and Peng Cui. Towards non-i.i.d. image classification: A dataset and baselines, 2019.
- [34] JB Heaton, Nicholas G Polson, and Jan Hendrik Witte. Deep learning in finance. *arXiv preprint arXiv:1602.06561*, 2016.
- [35] Dan Hendrycks and Thomas Dietterich. Benchmarking neural network robustness to common corruptions and perturbations. *arXiv preprint arXiv:1903.12261*, 2019.
- [36] Dan Hendrycks, Xiaoyuan Liu, Eric Wallace, Adam Dziedzic, Rishabh Krishnan, and Dawn Song. Pretrained transformers improve out-of-distribution robustness. *arXiv preprint arXiv:2004.06100*, 2020.
- [37] Dan Hendrycks, Steven Basart, Norman Mu, Saurav Kadavath, Frank Wang, Evan Dorundo, Rahul Desai, Tyler Zhu, Samyak Parajuli, Mike Guo, et al. The many faces of robustness: A critical analysis of out-of-distribution generalization. In *Proceedings of the IEEE/CVF International Conference on Computer Vision*, pages 8340–8349, 2021.
- [38] Dan Hendrycks, Kevin Zhao, Steven Basart, Jacob Steinhardt, and Dawn Song. Natural adversarial examples. In *Proceedings of the IEEE/CVF Conference on Computer Vision and Pattern Recognition*, pages 15262–15271, 2021.

- [39] Sepp Hochreiter and Jürgen Schmidhuber. Long short-term memory. *Neural computation*, 9(8):1735–1780, 1997.
- [40] Weihua Hu, Matthias Fey, Marinka Zitnik, Yuxiao Dong, Hongyu Ren, Bowen Liu, Michele Catasta, and Jure Leskovec. Open graph benchmark: Datasets for machine learning on graphs. *Advances in neural information processing systems*, 33:22118–22133, 2020.
- [41] Dieuwke Hupkes, Verna Dankers, Mathijs Mul, and Elia Bruni. Compositionality decomposed: how do neural networks generalise? *Journal of Artificial Intelligence Research*, 67:757–795, 2020.
- [42] Hassan Ismail Fawaz, Germain Forestier, Jonathan Weber, Lhassane Idoumghar, and Pierre-Alain Muller. Deep learning for time series classification: a review. *Data mining and knowledge discovery*, 33(4):917–963, 2019.
- [43] Joel Janai, Fatma Güney, Aseem Behl, Andreas Geiger, et al. Computer vision for autonomous vehicles: Problems, datasets and state of the art. *Foundations and Trends® in Computer Graphics and Vision*, 12(1–3): 1–308, 2020.
- [44] Daniel Jarrett, Jinsung Yoon, Ioana Bica, Zhaozhi Qian, Ari Ercole, and Mihaela van der Schaar. Clairvoyance: A pipeline toolkit for medical time series. In *International Conference on Learning Representations*, 2021. URL <https://openreview.net/forum?id=xnC8YwKUE3k>.
- [45] Vinay Jayaram and Alexandre Barachant. Moabb: trustworthy algorithm benchmarking for bcis. *Journal of neural engineering*, 15(6):066011, 2018.
- [46] John Jumper, Richard Evans, Alexander Pritzel, Tim Green, Michael Figurnov, Olaf Ronneberger, Kathryn Tunyasuvunakool, Russ Bates, Augustin Žídek, Anna Potapenko, et al. Highly accurate protein structure prediction with alphafold. *Nature*, 596(7873):583–589, 2021.
- [47] Bob Kemp, Aeilko H Zwinderman, Bert Tuk, Hilbert AC Kamphuisen, and Josefien JL Oberye. Analysis of a sleep-dependent neuronal feedback loop: the slow-wave microcontinuity of the eeg. *IEEE Transactions on Biomedical Engineering*, 47(9):1185–1194, 2000.
- [48] Daniel Keysers, Nathanael Schärli, Nathan Scales, Hylke Buisman, Daniel Furrer, Sergii Kashubin, Nikola Momchev, Danila Sinopalnikov, Lukasz Stafiniak, Tibor Tihon, et al. Measuring compositional generalization: A comprehensive method on realistic data. *arXiv preprint arXiv:1912.09713*, 2019.
- [49] Najoung Kim and Tal Linzen. Cogs: A compositional generalization challenge based on semantic interpretation. *arXiv preprint arXiv:2010.05465*, 2020.
- [50] Masanari Kimura, Takuma Nakamura, and Yuki Saito. Shift15m: Multiobjective large-scale fashion dataset with distributional shifts. *arXiv preprint arXiv:2108.12992*, 2021.
- [51] Pang Wei Koh, Shiori Sagawa, Henrik Marklund, Sang Michael Xie, Marvin Zhang, Akshay Balsubramani, Weihua Hu, Michihiro Yasunaga, Richard Lanus Phillips, Irena Gao, Tony Lee, Etienne David, Ian Stavness, Wei Guo, Berton A. Earnshaw, Imran S. Haque, Sara Beery, Jure Leskovec, Anshul Kundaje, Emma Pierson, Sergey Levine, Chelsea Finn, and Percy Liang. Wilds: A benchmark of in-the-wild distribution shifts, 2021.
- [52] Masanori Koyama and Shoichiro Yamaguchi. When is invariance useful in an out-of-distribution generalization problem? *arXiv preprint arXiv:2008.01883*, 2020.
- [53] Alex Krizhevsky, Ilya Sutskever, and Geoffrey E Hinton. Imagenet classification with deep convolutional neural networks. *Advances in neural information processing systems*, 25, 2012.
- [54] David Krueger, Ethan Caballero, Joern-Henrik Jacobsen, Amy Zhang, Jonathan Binas, Dinghuai Zhang, Remi Le Priol, and Aaron Courville. Out-of-distribution generalization via risk extrapolation (rex), 2021.
- [55] Brenden Lake and Marco Baroni. Generalization without systematicity: On the compositional skills of sequence-to-sequence recurrent networks. In *International conference on machine learning*, pages 2873–2882. PMLR, 2018.
- [56] Vernon J Lawhern, Amelia J Solon, Nicholas R Waytowich, Stephen M Gordon, Chou P Hung, and Brent J Lance. Eegnet: a compact convolutional neural network for eeg-based brain–computer interfaces. *Journal of neural engineering*, 15(5):056013, 2018.
- [57] Angeliki Lazaridou, Adhi Kuncoro, Elena Gribovskaya, Devang Agrawal, Adam Liska, Tayfun Terzi, Mai Gimenez, Cyprien de Masson d’Autume, Tomas Kocisky, Sebastian Ruder, et al. Mind the gap: Assessing temporal generalization in neural language models. *Advances in Neural Information Processing Systems*, 34, 2021.
- [58] Min-Ho Lee, O-Yeon Kwon, Yong-Jeong Kim, Hong-Kyung Kim, Young-Eun Lee, John Williamson, Siamac Fazli, and Seong-Wan Lee. Eeg dataset and openbmi toolbox for three bci paradigms: an investigation into bci illiteracy. *GigaScience*, 8(5):giz002, 2019.

- [59] Da Li, Yongxin Yang, Yi-Zhe Song, and Timothy M Hospedales. Deeper, broader and artier domain generalization. In *Proceedings of the IEEE international conference on computer vision*, pages 5542–5550, 2017.
- [60] Haoyang Li, Xin Wang, Ziwei Zhang, and Wenwu Zhu. Out-of-distribution generalization on graphs: A survey. *arXiv preprint arXiv:2202.07987*, 2022.
- [61] Bryan Lim and Stefan Zohren. Time-series forecasting with deep learning: a survey. *Philosophical Transactions of the Royal Society A*, 379(2194):20200209, 2021.
- [62] Evan Z Liu, Behzad Haghighi, Annie S Chen, Aditi Raghunathan, Pang Wei Koh, Shiori Sagawa, Percy Liang, and Chelsea Finn. Just train twice: Improving group robustness without training group information. In *International Conference on Machine Learning*, pages 6781–6792. PMLR, 2021.
- [63] Ziwei Liu, Ping Luo, Xiaogang Wang, and Xiaoou Tang. Deep learning face attributes in the wild. In *Proceedings of the IEEE international conference on computer vision*, pages 3730–3738, 2015.
- [64] Chaochao Lu, Yuhuai Wu, José Miguel Hernández-Lobato, and Bernhard Schölkopf. Nonlinear invariant risk minimization: A causal approach. *arXiv preprint arXiv:2102.12353*, 2021.
- [65] Andrew Maas, Raymond E Daly, Peter T Pham, Dan Huang, Andrew Y Ng, and Christopher Potts. Learning word vectors for sentiment analysis. In *Proceedings of the 49th annual meeting of the association for computational linguistics: Human language technologies*, pages 142–150, 2011.
- [66] Andrey Malinin, Neil Band, German Chesnokov, Yarin Gal, Mark JF Gales, Alexey Noskov, Andrey Ploskonosov, Liudmila Prokhorenkova, Ivan Provilkov, Vatsal Raina, et al. Shifts: A dataset of real distributional shift across multiple large-scale tasks. *arXiv preprint arXiv:2107.07455*, 2021.
- [67] Julian McAuley, Christopher Targett, Qinfeng Shi, and Anton Van Den Hengel. Image-based recommendations on styles and substitutes. In *Proceedings of the 38th international ACM SIGIR conference on research and development in information retrieval*, pages 43–52, 2015.
- [68] Manfred Mudelsee. Trend analysis of climate time series: A review of methods. *Earth-science reviews*, 190: 310–322, 2019.
- [69] Jens Müller, Robert Schmier, Lynton Ardizzone, Carsten Rother, and Ullrich Köthe. Learning robust models using the principle of independent causal mechanisms. In *DAGM German Conference on Pattern Recognition*, pages 79–110. Springer, 2021.
- [70] Bret Nestor, Matthew BA McDermott, Willie Boag, Gabriela Berner, Tristan Naumann, Michael C Hughes, Anna Goldenberg, and Marzyeh Ghassemi. Feature robustness in non-stationary health records: caveats to deployable model performance in common clinical machine learning tasks. In *Machine Learning for Healthcare Conference*, pages 381–405. PMLR, 2019.
- [71] Yonatan Oren, Shiori Sagawa, Tatsunori B Hashimoto, and Percy Liang. Distributionally robust language modeling. *arXiv preprint arXiv:1909.02060*, 2019.
- [72] Giambattista Parascandolo, Alexander Neitz, Antonio Orvieto, Luigi Gresele, and Bernhard Schölkopf. Learning explanations that are hard to vary. *arXiv preprint arXiv:2009.00329*, 2020.
- [73] Judea Pearl. Causal diagrams for empirical research. *Biometrika*, 82(4):669–688, 1995.
- [74] Judea Pearl. *Causality*. Cambridge university press, 2009.
- [75] Xingchao Peng, Qinxun Bai, Xide Xia, Zijun Huang, Kate Saenko, and Bo Wang. Moment matching for multi-source domain adaptation. In *Proceedings of the IEEE/CVF international conference on computer vision*, pages 1406–1415, 2019.
- [76] Jonas Peters, Peter Bühlmann, and Nicolai Meinshausen. Causal inference by using invariant prediction: identification and confidence intervals. *Journal of the Royal Statistical Society: Series B (Statistical Methodology)*, 78(5):947–1012, 2016.
- [77] Mohammad Pezeshki, Sékou-Oumar Kaba, Yoshua Bengio, Aaron Courville, Doina Precup, and Guillaume Lajoie. Gradient starvation: A learning proclivity in neural networks, 2021.
- [78] Stephen R Pfohl, Haoran Zhang, Yizhe Xu, Agata Foryciarz, Marzyeh Ghassemi, and Nigam H Shah. A comparison of approaches to improve worst-case predictive model performance over patient subpopulations. *Scientific reports*, 12(1):1–13, 2022.
- [79] Alvin Rajkomar, Eyal Oren, Kai Chen, Andrew M Dai, Nissan Hajaj, Michaela Hardt, Peter J Liu, Xiaobing Liu, Jake Marcus, Mimi Sun, et al. Scalable and accurate deep learning with electronic health records. *NPJ Digital Medicine*, 1(1):1–10, 2018.

- [80] Alexandre Rame, Corentin Dancette, and Matthieu Cord. Fishr: Invariant gradient variances for out-of-distribution generalization. *arXiv preprint arXiv:2109.02934*, 2021.
- [81] Muhammad Imran Razzak, Saeeda Naz, and Ahmad Zaib. Deep learning for medical image processing: Overview, challenges and the future. *Classification in BioApps*, pages 323–350, 2018.
- [82] Benjamin Recht, Rebecca Roelofs, Ludwig Schmidt, and Vaishaal Shankar. Do imagenet classifiers generalize to imagenet? In *International Conference on Machine Learning*, pages 5389–5400. PMLR, 2019.
- [83] Alexander Robey, George Pappas, and Hamed Hassani. Model-based domain generalization. *Advances in Neural Information Processing Systems*, 34, 2021.
- [84] Mateo Rojas-Carulla, Bernhard Schölkopf, Richard Turner, and Jonas Peters. A causal perspective on domain adaptation. *stat*, 1050:19, 2015.
- [85] Mateo Rojas-Carulla, Bernhard Schölkopf, Richard Turner, and Jonas Peters. Invariant models for causal transfer learning. *The Journal of Machine Learning Research*, 19(1):1309–1342, 2018.
- [86] Franco Ronchetti, Facundo Quiroga, César Armando Estrebow, Laura Cristina Lanzarini, and Alejandro Rosete. Lsa64: an argentinian sign language dataset. In *XXII Congreso Argentino de Ciencias de la Computación (CACIC 2016)*, 2016.
- [87] Elan Rosenfeld, Pradeep Ravikumar, and Andrej Risteski. Domain-adjusted regression or: Erm may already learn features sufficient for out-of-distribution generalization. *arXiv preprint arXiv:2202.06856*, 2022.
- [88] Yangjun Ruan, Yann Dubois, and Chris J Maddison. Optimal representations for covariate shift. *arXiv preprint arXiv:2201.00057*, 2021.
- [89] Shiori Sagawa, Pang Wei Koh, Tatsunori B. Hashimoto, and Percy Liang. Distributionally robust neural networks for group shifts: On the importance of regularization for worst-case generalization, 2020.
- [90] Shiori Sagawa, Pang Wei Koh, Tony Lee, Irena Gao, Sang Michael Xie, Kendrick Shen, Ananya Kumar, Weihua Hu, Michihiro Yasunaga, Henrik Marklund, et al. Extending the wilds benchmark for unsupervised adaptation. *arXiv preprint arXiv:2112.05090*, 2021.
- [91] Shibani Santurkar, Dimitris Tsipras, and Aleksander Madry. Breeds: Benchmarks for subpopulation shift. *arXiv preprint arXiv:2008.04859*, 2020.
- [92] David Saxton, Edward Grefenstette, Felix Hill, and Pushmeet Kohli. Analysing mathematical reasoning abilities of neural models. *arXiv preprint arXiv:1904.01557*, 2019.
- [93] Gerwin Schalk, Dennis J McFarland, Thilo Hinterberger, Niels Birbaumer, and Jonathan R Wolpaw. Bci2000: a general-purpose brain-computer interface (bci) system. *IEEE Transactions on biomedical engineering*, 51(6): 1034–1043, 2004.
- [94] Robin Tibor Schirrmester, Jost Tobias Springenberg, Lukas Dominique Josef Fiederer, Martin Glasstetter, Katharina Eggensperger, Michael Tangermann, Frank Hutter, Wolfram Burgard, and Tonio Ball. Deep learning with convolutional neural networks for eeg decoding and visualization. *Human Brain Mapping*, aug 2017. ISSN 1097-0193. doi: 10.1002/hbm.23730. URL <http://dx.doi.org/10.1002/hbm.23730>.
- [95] Bernhard Schölkopf, Francesco Locatello, Stefan Bauer, Nan Rosemary Ke, Nal Kalchbrenner, Anirudh Goyal, and Yoshua Bengio. Toward causal representation learning. *Proceedings of the IEEE*, 109(5):612–634, 2021.
- [96] Omer Berat Sezer, Mehmet Ugur Gudelek, and Ahmet Murat Ozbayoglu. Financial time series forecasting with deep learning: A systematic literature review: 2005–2019. *Applied soft computing*, 90:106181, 2020.
- [97] Soroosh Shahtalebi, Jean-Christophe Gagnon-Audet, Touraj Laleh, Mojtaba Faramarzi, Kartik Ahuja, and Irina Rish. Sand-mask: An enhanced gradient masking strategy for the discovery of invariances in domain generalization. *arXiv preprint arXiv:2106.02266*, 2021.
- [98] Hossein Sharifi-Noghabi, Parsa Alamzadeh Harjandi, Olga Zolotareva, Colin C Collins, and Martin Ester. Velodrome: Out-of-distribution generalization from labeled and unlabeled gene expression data for drug response prediction. *bioRxiv*, 2021.
- [99] Zheyang Shen, Jiashuo Liu, Yue He, Xingxuan Zhang, Renzhe Xu, Han Yu, and Peng Cui. Towards out-of-distribution generalization: A survey. *arXiv preprint arXiv:2108.13624*, 2021.
- [100] David Silver, Aja Huang, Chris J Maddison, Arthur Guez, Laurent Sifre, George Van Den Driessche, Julian Schrittwieser, Ioannis Antonoglou, Veda Panneershelvam, Marc Lanctot, et al. Mastering the game of go with deep neural networks and tree search. *nature*, 529(7587):484–489, 2016.

- [101] Richard Socher, Alex Perelygin, Jean Wu, Jason Chuang, Christopher D Manning, Andrew Y Ng, and Christopher Potts. Recursive deep models for semantic compositionality over a sentiment treebank. In *Proceedings of the 2013 conference on empirical methods in natural language processing*, pages 1631–1642, 2013.
- [102] Allan Stisen, Henrik Blunck, Sourav Bhattacharya, Thor Siiger Prentow, Mikkel Baun Kjærgaard, Anind Dey, Tobias Sonne, and Mads Møller Jensen. Smart devices are different: Assessing and mitigating mobile sensing heterogeneities for activity recognition. In *Proceedings of the 13th ACM conference on embedded networked sensor systems*, pages 127–140, 2015.
- [103] David S Stoffer and Hernando Ombao. Special issue on time series analysis in the biological sciences, 2012.
- [104] Eric V Strobl, Kun Zhang, and Shyam Visweswaran. Approximate kernel-based conditional independence tests for fast non-parametric causal discovery. *Journal of Causal Inference*, 7(1), 2019.
- [105] Akinori Tanaka, Akio Tomiya, and Kōji Hashimoto. *Deep Learning and Physics*. Springer, 2021.
- [106] Mario Giovanni Terzano, Liborio Parrino, Adriano Sherieri, Ronald Chervin, Sudhansu Chokroverty, Christian Guilleminault, Max Hirshkowitz, Mark Mahowald, Harvey Moldofsky, Agostino Rosa, et al. Atlas, rules, and recording techniques for the scoring of cyclic alternating pattern (cap) in human sleep. *Sleep medicine*, 2(6): 537–553, 2001.
- [107] Eric J Topol. High-performance medicine: the convergence of human and artificial intelligence. *Nature medicine*, 25(1):44–56, 2019.
- [108] Antonio Torralba and Alexei A Efros. Unbiased look at dataset bias. In *CVPR 2011*, pages 1521–1528. IEEE, 2011.
- [109] José F Torres, Dalil Hadjout, Abderrazak Sebaa, Francisco Martínez-Álvarez, and Alicia Troncoso. Deep learning for time series forecasting: a survey. *Big Data*, 9(1):3–21, 2021.
- [110] Vladimir N. Vapnik. *Statistical Learning Theory*. Wiley-Interscience, 1998.
- [111] Ashish Vaswani, Noam Shazeer, Niki Parmar, Jakob Uszkoreit, Llion Jones, Aidan N Gomez, Łukasz Kaiser, and Illia Polosukhin. Attention is all you need. *Advances in neural information processing systems*, 30, 2017.
- [112] Hemanth Venkateswara, Jose Eusebio, Shayok Chakraborty, and Sethuraman Panchanathan. Deep hashing network for unsupervised domain adaptation. In *Proceedings of the IEEE conference on computer vision and pattern recognition*, pages 5018–5027, 2017.
- [113] Haohan Wang, Songwei Ge, Zachary Lipton, and Eric P Xing. Learning robust global representations by penalizing local predictive power. *Advances in Neural Information Processing Systems*, 32, 2019.
- [114] Simeon Warner. Open archives initiative protocol development and implementation at arxiv. *arXiv preprint cs/0101027*, 2001.
- [115] Qingsong Wen, Liang Sun, Fan Yang, Xiaomin Song, Jingkun Gao, Xue Wang, and Huan Xu. Time series data augmentation for deep learning: A survey. *arXiv preprint arXiv:2002.12478*, 2020.
- [116] Adina Williams, Nikita Nangia, and Samuel R Bowman. A broad-coverage challenge corpus for sentence understanding through inference. *arXiv preprint arXiv:1704.05426*, 2017.
- [117] Ho Yuen Frank Wong, Hiu Yin Sonia Lam, Ambrose Ho-Tung Fong, Siu Ting Leung, Thomas Wing-Yan Chin, Christine Shing Yen Lo, Macy Mei-Sze Lui, Jonan Chun Yin Lee, Keith Wan-Hang Chiu, Tom Wai-Hin Chung, et al. Frequency and distribution of chest radiographic findings in patients positive for covid-19. *Radiology*, 296(2):E72–E78, 2020.
- [118] Kai Xiao, Logan Engstrom, Andrew Ilyas, and Aleksander Madry. Noise or signal: The role of image backgrounds in object recognition. *arXiv preprint arXiv:2006.09994*, 2020.
- [119] Yilun Xu and Tommi Jaakkola. Learning representations that support robust transfer of predictors. *arXiv preprint arXiv:2110.09940*, 2021.
- [120] Sijie Yang, Fei Zhu, Xinghong Ling, Quan Liu, and Peiyao Zhao. Intelligent health care: Applications of deep learning in computational medicine. *Frontiers in Genetics*, 12:444, 2021.
- [121] Haotian Ye, Chuanlong Xie, Tianle Cai, Ruichen Li, Zhenguo Li, and Liwei Wang. Towards a theoretical framework of out-of-distribution generalization. *Advances in Neural Information Processing Systems*, 34, 2021.
- [122] Nanyang Ye, Kaican Li, Lanqing Hong, Haoyue Bai, Yiting Chen, Fengwei Zhou, and Zhenguo Li. Ood-bench: Benchmarking and understanding out-of-distribution generalization datasets and algorithms, 2021.
- [123] Haoran Zhang, Natalie Dullerud, Laleh Seyyed-Kalantari, Quaid Morris, Shalmali Joshi, and Marzyeh Ghassemi. An empirical framework for domain generalization in clinical settings. In *Proceedings of the Conference on Health, Inference, and Learning*, pages 279–290, 2021.

- [124] Kun Zhang, Jonas Peters, Dominik Janzing, and Bernhard Schölkopf. Kernel-based conditional independence test and application in causal discovery. *arXiv preprint arXiv:1202.3775*, 2012.
- [125] Sheng Zhang, Xiaodong Liu, Jingjing Liu, Jianfeng Gao, Kevin Duh, and Benjamin Van Durme. Record: Bridging the gap between human and machine commonsense reading comprehension. *arXiv preprint arXiv:1810.12885*, 2018.

## A Additional dataset information

### A.1 Spurious-Fourier

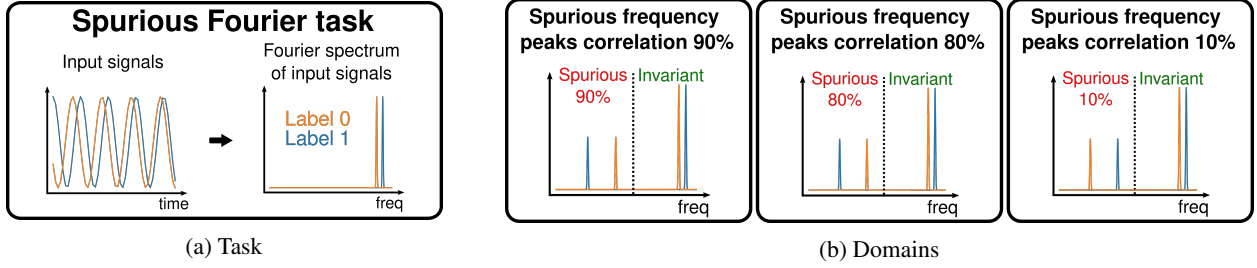


Figure 13: Description of the Spurious-Fourier dataset

#### A.1.1 Setup

**Motivation** Recall the cow or camel classification problem from Section 1, where a deep learning model trained to distinguish cows from camels learns to rely on the background properties (e.g., grass or sand) instead of the animal characteristic features (e.g., color and shape) to make a prediction. Arjovsky et al. [5] proposed Colored MNIST (CMNIST) to recreate the the cow or camel classification problem into a simple benchmark in the image domain. In the Spurious-Fourier dataset, we adapt this same problem in the time series setting.

**Problem setting** We create a dataset composed of one-dimensional signals, where the task is to perform binary classification based on the frequency characteristics. Signals are constructed from Fourier spectrums with one low-frequency peak ( $L$ ) and one high-frequency peak ( $H$ ). The low-frequency peak is one of the two possible frequencies ( $L_A$  or  $L_B$ ), and the high-frequency peak is also one of two possible frequencies ( $H_A$  or  $H_B$ ), see Figure 3. Domains  $D^d |_{d \in \{10\%, 80\%, 90\%\}}$  contain signal-label pairs, where the label is a noisy function of the low- and high-frequencies such that low-frequency peaks bear a varying correlation of  $d$  with the label and high-frequency peaks bear an invariant correlation of 75% with the label

**Data** We first create four Fourier spectra with all combinations of low and high frequency peaks. From that, we perform the inverse Fourier transform to get one long 1 dimensional signal for each of those spectra. We then split this long signal into smaller sequences of half a second totaling 50 time-steps. We then recreate the Colored MNIST [5] dataset characteristic. We first add 25% label noise to the labels by flipping the labels by using a Bernoulli distribution of parameter  $p = 0.25$ . We then build the domains by gathering 2000 signals with the noisy label 0 and 2000 signals with the noisy label 1. For every signal we add to a domain, we sample a value from a Bernoulli distribution of parameters  $p$  equal to the domain definition (10%, 80% or 90%) and pick a signal with a spurious frequency peak at 2Hz if we sample 0 or a signal with a spurious frequency peak at 4Hz if we sample 1. This way we create correlation with the label and the spurious frequency peak following the domain definition.

**Domain information** Here we find the distribution of data samples and their labels domain by domain.

Domain	8.5Hz	9Hz	Total
10%	2043	1957	4000
80%	2013	1987	4000
90%	1991	2009	4000
<b>Total</b>	<b>6047</b>	<b>5953</b>	<b>12000</b>

Table 5: Domain proportions of labels in the Spurious-Fourier Dataset

**Architecture choice** For this simple task, we use the LSTM [39] model because it is a simple model well accepted in the time series/sequential prediction field. We stack on top of the LSTM a fully connected (FC) layer used to make predictions at the last time step of the time series. Layers are detailed in Table 6



#	Layer
15	LSTM(in=1, hidden_size=20, num_layers=2)
16	Linear(in=20, out=20)
17	ReLU
18	Linear(in=20, out=2)

Table 6: Model architecture used for the Spurious-Fourier dataset

### A.1.2 Detailed results

**Oracle task** In the WOODS repository, we also provide the Basic Fourier dataset. It is the same task as Spurious-Fourier, but without any label noise and spurious frequency peaks. This is not a domain generalization task, but instead acts as a proof of concept that the underlying invariant task is possible with the model and setup we are using.

Objective	no spur	Average
ID ERM	100.00 $\pm$ 0.00	100.00

Table 7: ID results for the Basic Fourier dataset

**ID evaluation** We evaluate the performance of ERM when it has access to all domains. Columns correspond to the validation accuracy of each domain of a single training run determined by the train-domain validation model selection method. We see that in learns, as expected, the invariant solution to the task.

Algorithm	10%	80%	90%	Average
ID ERM	74.46 $\pm$ 0.07	74.79 $\pm$ 0.03	73.54 $\pm$ 0.07	74.26

Table 8: ID results for the Spurious-Fourier dataset

**Baseline evaluations** We evaluate our baseline performance on the dataset. We evaluate the performance only when holding out the 10% domain as it is the only domain of meaning, and including the other domains only dilutes the information carried by this dataset.

train-domain validation			Test-domain validation		
Objective	10%	Average	Objective	10%	Average
ID ERM	74.46 $\pm$ 0.07	74.46	ID ERM	74.46 $\pm$ 0.07	74.46
ERM	9.75 $\pm$ 0.23	9.75	ERM	9.30 $\pm$ 0.07	9.30
VREx	9.77 $\pm$ 0.20	9.77	VREx	65.39 $\pm$ 4.84	65.39
IRM	9.35 $\pm$ 0.09	9.35	IRM	57.68 $\pm$ 0.84	57.68
SD	10.28 $\pm$ 0.16	10.28	SD	9.25 $\pm$ 0.03	9.25
IB-ERM	10.08 $\pm$ 0.37	10.08	IB-ERM	9.28 $\pm$ 0.05	9.28

Table 9: Baseline results for the Spurious-Fourier dataset

## A.2 Temporal Colored MNIST

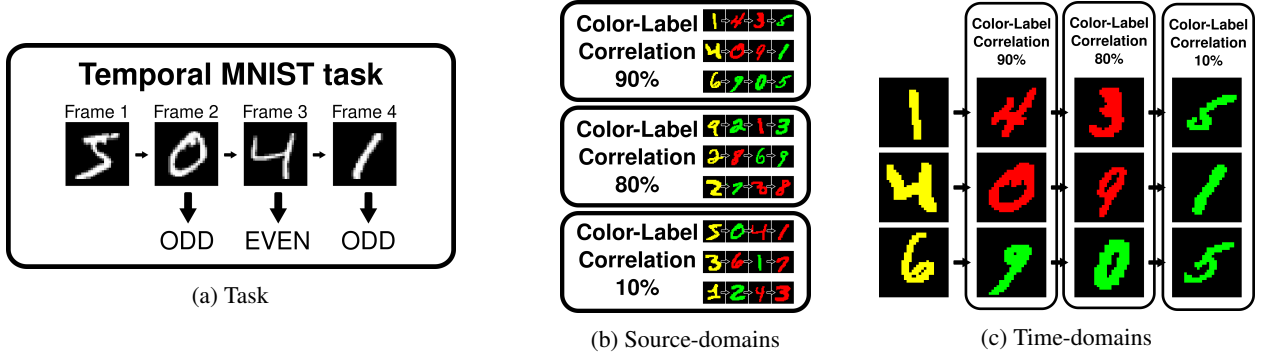


Figure 14: Description of the Temporal Colored MNIST dataset

### A.2.1 Setup

**Motivation** In light of the previously mentioned cow or camel classification problem, Arjovsky et al. [5] proposed the CMNIST dataset as a synthetic investigation of this problem. We propose an extension of this widely used dataset to time series, where we explore new domain formulations in multiple prediction (Section 3.2.2) tasks.

**Problem setting** In Temporal Colored MNIST (TCMNIST), we create a binary classification task of video frames. Videos are sequences of four MNIST digits where the goal is to predict whether the sum of the current and previous digits in the sequence is odd or even, see Figure 5. Prediction is made for all frames except for the first one. We use this one task definition to investigate both domain definition paradigms presented in Section 3.2: Source-domains (Example 3.2) and Time-domains (Example 3.3).

**Data** We create the dataset using the MNIST digits, which we concatenate into sequences and attribute labels according to the parity task. We then add spuriousness to the data by following the setup of Colored MNIST [5]. We first add 25% label noise by flipping the labels using a Bernoulli distribution of parameter  $p = 0.25$ . We then add color to the grey images by taking the noisy labels and flipping them following a Bernoulli distribution of parameter,  $p$  equals to the domain definition (10%, 80%, 90%), and color the digit red is the flipped noisy label is 0 or green if the flipped noisy label is 1. In the case of **TCMNIST-Source**, whole sequences of digit belongs to the same domain, therefore the Bernoulli parameter  $p$  will stay constant throughout the sequence, but might change from sequence to sequence depending if the domain is changing. In **TCMNIST-Time**, the correlation value changes throughout the sequence, but all samples have the same correlation pattern. The Bernoulli parameter  $p$  changes in the sequence.

**Domain information** Here we detail the distribution of data samples and their label domain by domain

TCMNIST-Source				TCMNIST-Time			
Domain	Even	Odd	Domain Total	Domain	Even	Odd	Domain Total
10%	8603	8899	17502	10%	8564	8936	17500
80%	8583	8916	17499	80%	8765	8735	17500
90%	8563	8936	17499	90%	8613	8887	17500
<b>Total</b>	<b>25749</b>	<b>26751</b>	<b>52500</b>	<b>Total</b>	<b>25942</b>	<b>26558</b>	<b>52500</b>

Table 10: Domain proportions of labels in both Temporal Colored MNIST Dataset

**Architecture choice** For this task, we use a combination of a CNN and an LSTM architecture. Table 11 details the layers of the model architecture. Its parameters were hand tuned to perform well on this toy task.

#	Layer
1	Conv2D(in=d, out=8, padding=1)
2	ReLU
3	Conv2D(in=8, out=32, stride=2, padding=1)
4	ReLU
5	MaxPool2d
6	Conv2D(in=32, out=32, padding=1)
7	ReLU
8	MaxPool2d
9	Conv2D(in=32, out=32, padding=1)
10	ReLU
11	Linear(in=288, out=64)
12	ReLU
13	Linear(in=64, out=32)
14	ReLU
15	LSTM(in=32, hidden_size=128, num_layers=1)
16	Linear(in=128, out=64)
17	ReLU
16	Linear(in=64, out=64)
17	ReLU
18	Linear(in=64, out=2)

Table 11: Model architecture used for both Temporal Colored MNIST dataset

### A.2.2 Detailed results

**Oracle task** In the WOODS repository, we also provide the Temporal MNIST dataset. It is the same task as both the Temporal Colored MNIST datasets, but colors are not present. This is not a domain generalization task, but instead acts as a proof that the underlying task of classifying odd or even sums of digits in this context is possible.

Objective	grey	Average
ID ERM	$98.77 \pm 0.02$	98.77

Table 12: ID results for the Temporal MNIST dataset

**ID evaluation** We show the ID results of ERM for both the Temporal Colored MNIST dataset in Table 13 and Table 14. We obtain these results by doing a hyperparameter search with the methodology detailed in Appendix D, but with no held-out test domain. In other words, all the domains are ID. We then perform train-domain validation to choose the best performing model and report its accuracy.

Algorithm	10%	80%	90%	Average
ID ERM	$68.36 \pm 0.13$	$73.49 \pm 0.13$	$74.85 \pm 0.16$	72.23

Table 13: ID results for the TCMNIST-Source dataset

Algorithm	10%	80%	90%	Average
ID ERM	$89.97 \pm 0.00$	$80.98 \pm 0.02$	$91.20 \pm 0.00$	87.38

Table 14: ID results for the TCMNIST-Time dataset

Train-domain validation			Test-domain validation		
Algorithm	10%	Average	Algorithm	10%	Average
ID ERM	$68.36 \pm 0.13$	68.36	ID ERM	$68.36 \pm 0.13$	68.36
VREx	$10.00 \pm 0.01$	10.00	VREx	$50.39 \pm 0.34$	50.39
ERM	$10.15 \pm 0.13$	10.15	ERM	$27.37 \pm 2.09$	27.37
IRM	$9.98 \pm 0.00$	9.98	IRM	$52.11 \pm 1.24$	52.11
SD	$10.01 \pm 0.01$	10.01	SD	$24.12 \pm 3.33$	24.12
IB-ERM	$10.00 \pm 0.01$	10.00	IB-ERM	$50.61 \pm 0.00$	50.61

Table 15: Baseline results for the TCMNIST-Source dataset

Train-domain validation			Test-domain validation		
Algorithm	10%	Average	Algorithm	10%	Average
ID ERM	$89.97 \pm 0.00$	89.97	ID ERM	$89.97 \pm 0.00$	89.97
ERM	$10.04 \pm 0.00$	10.04	ERM	$25.78 \pm 4.70$	25.78
VREx	$10.05 \pm 0.00$	10.05	VREx	$36.91 \pm 10.98$	36.91
IRM	$10.04 \pm 0.00$	10.04	IRM	$53.66 \pm 2.14$	53.66
SD	$10.05 \pm 0.00$	10.05	SD	$22.06 \pm 3.21$	22.06
IB-ERM	$10.05 \pm 0.01$	10.05	IB-ERM	$24.71 \pm 1.58$	24.71

Table 16: Baseline results for the TCMNIST-Time dataset

## Baseline evaluations

### A.3 CAP

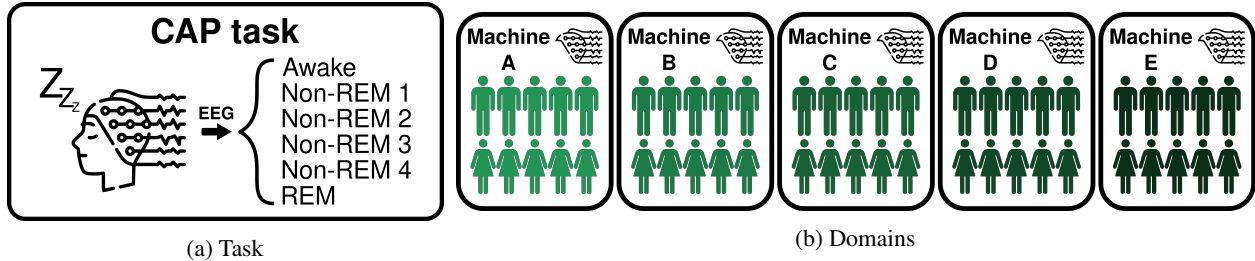


Figure 15: Description of the CAP dataset

#### A.3.1 Setup

**Motivation** A recurrent problem in computational medicine is that models trained on data from a given recording machine will not generalize to data coming from another machine, even when both machines are from a similar constructor. Failure to generalize to unseen machines can cause critical issues for clinical practice because a false sense of confidence in a model could lead to a false diagnosis. Furthermore, even when following the exact same data gathering procedures, a change in the recording machinery can lead to catastrophic distributional shifts. We study these machinery-induced distribution shifts with the CAP dataset.

**Problem setting** We consider the sleep stage classification task from electroencephalographic (EEG) measurements. The labels are six sleep stages (i.e., Awake, Non-REM 1-2-3-4, and REM) labeled by experts in the field. The data comes from five different machines, which act as our five Source-domains. The goal is to generalize to unseen machines. As a whole, the dataset is composed of 40390 recordings of 30 seconds each from 19 EEG channels gathered on 41 participants.

**Data** The dataset consists of 40390 sequences of EEG recordings taken from about 41 full nights of sleep of 41 participants taken on 5 machines. Concretely, the inputs  $x$  are multivariate time series that take the form of 19 channels and 3000 time steps sampled at 100Hz. The 19 channels mostly contain EEG measurements but include Electromyography (EMG) measurements, Electrocardiography (ECG) measurements, and heart rate measurements. They are sequences of 30 seconds in length, a standard sequence length for the task of sleep stage classification. Data gathered by different machines originate from disjoint sets of participants. The labels  $y$  consist of 6 sleep stages: Awake, Non-REM 1, Non-REM 2, Non-REM 3, Non-REM 4, and REM. The domains  $d$  are the 5 EEG machines: Machine A, Machine B, Machine C, Machine D, and Machine E. The 19 channels are shared between the different machines: dx1-dx2, f4-c4, fp1-f3, emg1-emg2, ecg1-ecg2, roc-loc, f8-t4, fp2-f4, p3-o1, pleth, hr, c4-a1, p4-a1, p4-o2, c4-p4, f7-t3, sao2, sx1-sx2, f3-c3, and c3-p3. Concretely, the inputs are multivariate time series that take the form of 19 channels and 3000 time steps sampled at 100Hz.

**Preprocessing** This section details the preprocessing steps taken to bring the CAP dataset from its raw form to its final form used in WOODS. The rawCAP dataset contains data from 15 machines, each with different channels and sampling frequency characteristics. We choose the five machines with the most data, allowing us to have a good number (19) of shared channels between them. Next, we resample the data to a standard sampling frequency of 100Hz for all five machines. We then apply a bandpass filter from 0.3Hz to 30Hz. This bandpass filter removes frequency bands generally regarded as uninformative for sleep stage classification. We then detrend the data and normalize the data with a standard scaler applied to the channels individually. Finally, we split the multiple-hour entire time series of sleep into shorter sequences of 30 seconds for training.

**Domain information** The data from the different machines consists of data from disjoint sets of participants. Table 17 details the number of participants per domain and some demographic information; each had a single night of sleep recorded. Table 18 details the proportion of samples and labels across domains.

Domain	Number of participants	Male	Female	Age
Machine A	13	7	6	$33.1 \pm 13.9$
Machine B	5	5	0	$26.4 \pm 8.2$
Machine C	5	4	1	$73.4 \pm 6.42$
Machine D	10	5	5	$30.7 \pm 8.9$
Machine E	8	3	5	$36.8 \pm 16.7$
<b>Total</b>	41	24	17	$37.3 \pm 18.1$

Table 17: Number of participants and demographic information of the CAP Dataset

Domain	Awake	Non-REM 1	Non-REM 2	Non-REM 3	Non-REM 4	REM	Domain Total
Machine A	1448	350	4986	1533	2110	2342	12769
Machine B	318	171	1933	595	706	971	4694
Machine C	1318	294	1168	595	810	547	4732
Machine D	1114	580	3547	1273	1606	1810	9930
Machine E	967	276	3377	711	1251	1683	8265
<b>Total</b>	5165	1671	15011	4707	6483	7353	40390

Table 18: Domain proportions of labels in the CAP Dataset

**Architecture choice** For this dataset, we use a deep convolution network model as defined in work from Schirrmester et al. [94]. We use the implementation of the BrainDecode Schirrmester et al. [94] Toolbox. We chose this model because it is the perfect combination of performance stability and recognition from the EEG community.

### A.3.2 Detailed results

In this section, we detail the results obtained by our baselines algorithms (see Section 7).

**ID evaluation** We show the results of ERM for the CAP dataset in Table 19. We obtain these results by doing a hyperparameter search with the methodology detailed in Appendix D, but with no held-out test domain. In other words, all the domains are ID. We then perform train-domain validation to choose the best performing model and report its accuracy.

Algorithm	Machine A	Machine B	Machine C	Machine D	Machine E	Average
ID ERM	$78.26 \pm 0.52$	$78.14 \pm 1.00$	$63.39 \pm 1.38$	$78.73 \pm 0.34$	$77.09 \pm 0.37$	75.12

Table 19: ID results for the CAP dataset

**Baseline evaluation** We show the results of our set of baseline algorithms on the CAP dataset in Table 20. We obtain these results taking every domain as a held-out test set and performing a hyperparameter search with the methodology detailed in Appendix D. Hence, each column of Table 20 corresponds to the domain performance when taken as a test set.

Train-domain validation						
Objective	Machine A	Machine B	Machine C	Machine D	Machine E	Average
ID ERM	$78.26 \pm 0.52$	$78.14 \pm 1.00$	$63.39 \pm 1.38$	$78.73 \pm 0.34$	$77.09 \pm 0.37$	75.12
ERM	$68.70 \pm 0.58$	$64.00 \pm 0.17$	$40.10 \pm 0.27$	$72.03 \pm 0.26$	$68.35 \pm 0.56$	62.63
IB-ERM	$69.01 \pm 0.45$	$63.53 \pm 0.85$	$40.52 \pm 0.84$	$71.79 \pm 0.32$	$69.16 \pm 0.64$	62.80
IRM	$63.44 \pm 1.08$	$55.40 \pm 1.53$	$39.62 \pm 0.54$	$67.90 \pm 0.68$	$65.64 \pm 1.19$	58.40
SD	$69.29 \pm 0.25$	$55.53 \pm 1.45$	$41.36 \pm 1.78$	$71.14 \pm 0.22$	$66.48 \pm 0.92$	60.76
VREx	$64.49 \pm 0.42$	$51.98 \pm 2.62$	$38.96 \pm 0.42$	$68.39 \pm 0.71$	$63.53 \pm 0.22$	57.47
Oracle train-domain validation						
Objective	Machine A	Machine B	Machine C	Machine D	Machine E	Average
ID ERM	$78.26 \pm 0.52$	$78.14 \pm 1.00$	$63.39 \pm 1.38$	$78.73 \pm 0.34$	$77.09 \pm 0.37$	75.12
ERM	$69.62 \pm 0.40$	$65.23 \pm 0.45$	$43.01 \pm 0.87$	$72.47 \pm 0.29$	$69.69 \pm 0.61$	64.00
IB-ERM	$69.47 \pm 0.40$	$65.74 \pm 0.82$	$43.18 \pm 0.64$	$72.06 \pm 0.24$	$69.47 \pm 0.49$	63.98
IRM	$63.99 \pm 0.98$	$58.54 \pm 1.06$	$41.43 \pm 0.94$	$68.24 \pm 0.88$	$67.00 \pm 0.67$	59.84
SD	$69.38 \pm 0.20$	$61.84 \pm 0.39$	$43.97 \pm 1.09$	$71.41 \pm 0.14$	$69.41 \pm 0.29$	63.20
VREx	$64.49 \pm 0.42$	$55.26 \pm 0.84$	$39.38 \pm 0.18$	$68.40 \pm 0.71$	$63.58 \pm 0.21$	58.22

Table 20: Baseline results for the CAP dataset

### A.3.3 Credit and license

This dataset is adapted from the work of Terzano et al. [106], as made available on the online Physionet [28] platform. This dataset is licensed under the Open Data Commons Attribution License v1.0.

#### A.4 SEDFx



Figure 16: Description of the SEDFx dataset

##### A.4.1 Setup

**Motivation** In clinical settings, we train a model on the data gathered from a limited number of patients and hope this model will generalize to unseen patients in the future [78]. However, this generalization between observed patients in the training dataset and new patients at the test time is not guaranteed. Distributional shifts caused by shifts in patient demographics (e.g., age, gender, and ethnicity) can cause the model to fail. We study these patient demographic shifts with the SEDFx dataset.

**Problem setting** We consider the sleep classification task from EEG measurements. The labels are six sleep stages (Awake, Non-REM 1-2-3-4, and REM) labeled by experts in the field. The data comes from five age groups, which act as our Source-domains. The goal is to generalize to an unseen age demographic. As a whole, the dataset is composed of 238712 recordings of 30 seconds each from four EEG channels gathered on 100 participants.

**Data** The dataset consists of 238712 sequences of EEG recordings taken from about 200 full nights of sleep of 100 participants. Concretely, the inputs  $x$  are multivariate time series that take the form of 4 channels and 3000 time steps sampled at 100Hz. The four channels contain 2 EEG channels, 1 Electromyography (EOG) channel, and 1 Electrocardiography (ECG) channel. Those four channels are fpz-cz, pz-oz, EMG submental, EOG horizontal. Sequences are 30 seconds in length, a standard sequence length for the task of sleep stage classification. Data gathered by different machines originate from disjoint sets of participants. The labels  $y$  consist of 6 sleep stages: Awake, Non-REM 1, Non-REM 2, Non-REM 3, Non-REM 4, and REM. Domains  $d$  are the four disjoint age groups: Age 20-40, Age 40-60, Age 60-80, and age 80-100.

**Preprocessing** This section details the preprocessing steps taken to bring the SEDFx dataset from its raw form to its final form used in WOODS. The rawSEDFx dataset contains data from 2 machines, both with different channels and sampling frequency characteristics. We use the data from those two machines and use the four channels they have in common. Next, we resample the data to a standard sampling frequency of 100Hz for both machines. We then apply a bandpass filter from 0.3Hz to 30Hz. This bandpass filter removes frequency bands generally regarded as uninformative for sleep stage classification. Next, we crop the unlabeled onset and end of the complete recordings. Next, we split the multiple-hour entire time series of sleep into shorter sequences of 30 seconds for training. Finally, we then detrend the data and normalize the data with a standard scaler, applied to channels individually.

**Domain information** The data from the different machines consists of data from disjoint sets of participants. Table 22 details the number of participants per domain and some demographic information; most of which had two nights of sleep recorded. Table 22 details the proportion of samples and labels across domains.

Domain	Number of participants	Male	Female	Age
Age 20-40	32	14	18	$27.6 \pm 4.7$
Age 40-60	29	12	17	$53.3 \pm 3.4$
Age 60-80	23	10	13	$69.2 \pm 3.5$
Age 80-100	16	8	8	$90.5 \pm 4.5$
<b>Total</b>	100	44	56	$54.7 \pm 22.6$

Table 21: Number of participants and demographic information of the SEDFx Dataset

Domain	Awake	Non-REM 1	Non-REM 2	Non-REM 3	Non-REM 4	REM	Domain Total
Age 20-40	10505	4222	28105	4830	4254	12348	64264
Age 40-60	20405	7182	27222	3243	1423	10007	69482
Age 60-80	14708	7087	19186	2830	1400	6917	52128
Age 80-100	25358	6684	14410	1288	186	4912	52838
<b>Total</b>	70976	25175	88923	12191	7263	34184	238712

Table 22: Domain proportions of labels in the SEDFx Dataset

**Architecture choice** For this dataset, we use a deep convolution network model as defined in work from Schirrmester et al. [94]. We use the implementation of the BrainDecode Schirrmester et al. [94] Toolbox. We chose this model because it is the perfect combination of performance, stability, and recognition from the EEG community.

#### A.4.2 Detailed results

In this section, we detail the results obtained by our baselines algorithms (see Section 7).

**ID evaluation** We show the ID results of ERM for the SEDFx dataset in Table 23. We obtain these results by doing a hyperparameter search with the methodology detailed in Appendix D, but with no held-out test domain. In other words, all the domains are ID. We then perform train-domain validation to choose the best performing model and report its accuracy.

Algorithm	Age 20-40	Age 40-60	Age 60-80	Age 80-100	Average
ID ERM	$74.11 \pm 0.12$	$74.19 \pm 0.47$	$72.39 \pm 0.41$	$69.22 \pm 0.49$	72.48

Table 23: ID results for the SEDFx dataset

**Baseline evaluation** We show the results of our set of baseline algorithms on the SEDFx dataset in Table 24. We obtain these results taking every domain as a held-out test set and performing a hyperparameter search with the methodology detailed in Appendix D. Hence, each column of Table 24 corresponds to the domain performance when taken as a test set.



Train-domain validation					
Objective	Age 20-40	Age 40-60	Age 60-80	Age 80-100	Average
ID ERM	74.11 $\pm$ 0.12	74.19 $\pm$ 0.47	72.39 $\pm$ 0.41	69.22 $\pm$ 0.49	72.48
ERM	69.26 $\pm$ 1.12	71.45 $\pm$ 0.37	69.95 $\pm$ 0.23	66.46 $\pm$ 1.72	69.28
IB-ERM	69.41 $\pm$ 0.12	72.58 $\pm$ 0.46	69.79 $\pm$ 0.42	66.16 $\pm$ 0.87	69.48
IRM	62.46 $\pm$ 0.70	66.15 $\pm$ 0.37	62.07 $\pm$ 0.35	59.45 $\pm$ 0.71	62.53
SD	69.87 $\pm$ 1.34	73.18 $\pm$ 0.19	69.14 $\pm$ 0.16	67.18 $\pm$ 0.26	69.84
VREx	54.64 $\pm$ 0.85	63.79 $\pm$ 0.44	58.94 $\pm$ 0.41	54.52 $\pm$ 0.47	57.97

---

Oracle train-domain validation					
Objective	Age 20-40	Age 40-60	Age 60-80	Age 80-100	Average
ID ERM	74.11 $\pm$ 0.12	74.19 $\pm$ 0.47	72.39 $\pm$ 0.41	69.22 $\pm$ 0.49	72.48
ERM	71.11 $\pm$ 0.10	72.68 $\pm$ 0.43	70.07 $\pm$ 0.14	68.60 $\pm$ 1.22	70.61
IB-ERM	70.42 $\pm$ 0.41	72.79 $\pm$ 0.62	70.25 $\pm$ 0.12	69.08 $\pm$ 0.56	70.64
IRM	63.50 $\pm$ 0.02	66.37 $\pm$ 0.34	62.62 $\pm$ 0.16	60.43 $\pm$ 0.74	63.23
SD	71.22 $\pm$ 0.60	73.18 $\pm$ 0.19	69.60 $\pm$ 0.04	68.41 $\pm$ 0.60	70.60
VREx	56.22 $\pm$ 0.15	63.79 $\pm$ 0.44	58.94 $\pm$ 0.41	58.20 $\pm$ 0.22	59.29

Table 24: Baseline results for the SEDFx dataset

### A.4.3 Credit and license

This dataset was adapted from the work of Kemp et al. [47], as made available on the online Physionet [28] platform. This dataset is licensed under the Open Data Commons Attribution license v1.0.

## A.5 PCL

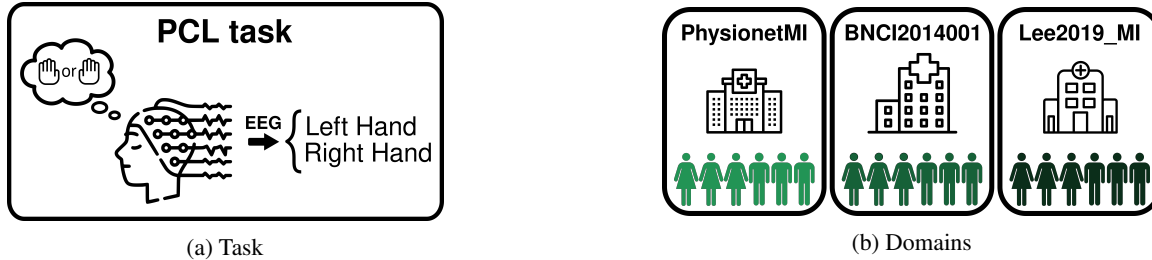


Figure 17: Description of the PCL dataset

### A.5.1 Setup

**Motivation** Aside from changes in the recording device and shifts in patient demographics, human intervention in the data gathering process is another contributing factor to the distributional shift that can lead to failure of clinical models. Specifically, a small change in the data-gathering procedures can cause procedural shifts that cause models to fail to generalize to other data gathering procedures. One known instance of this failure mode is the Camelyon17 [51] dataset, where models fail to generalize to other hospitals because of differences in the staining procedure of lymph node slices. This challenge is especially prevalent in temporal medical data (e.g., EEG, MEG, and others) because recording devices are complex tools greatly affected by nonlinear effects and modulations. These effects are often caused by context and preparations made before the recording [24]. We study these procedural shifts on the PCL dataset.

**Problem setting** We consider the motor imagery task from electroencephalographic (EEG) measurements. The labels are two imagined movements (left hand and right hand). The dataset comes from three different hospitals performing the same task under different data gathering procedures and conditions. They act as our Source-domains. The goal is

to generalize to unseen data gathering processes. As a whole, the dataset is composed of 22598 recordings of three seconds each from 48 EEG channels gathered with 215 participants.

**Data** The dataset consists of 22598 sequences of EEG recordings taken from 215 participants all doing the same task motor imagery task in different studies. Concretely, the inputs  $x$  are multivariate time series that take the form of 48 channels and 750 time steps sampled at 250Hz. The 48 channels contain only EEG measurements. Sequences are 3 seconds in length, which covers the full time of a single trial of the motor imagery task for the participants. Data gathered by different machines originate from disjoint sets of participants. The labels  $y$  consist of 2 imagery labels: left hand and right hand. Domains  $d$  are the 3 datasets from 3 different research institutions: PhysionetMI, Cho2017, Lee2019\_MI. The 48 channels are: AF7, CP5, AF4, P4, P8, P2, FC6, Fz, C5, O1, Fp1, Fp2, F4, CP4, PO3, C1, FC1, T8, Pz, Oz, TP7, Cz, FC2, CP6, CP2, POz, PO4, C6, P7, AF3, FC4, TP8, CP1, O2, C2, F8, FC3, P3, AF8, FC5, F7, F3, T7, C4, CP3, CPz, C3, P1. The channel locations are shown in Figure 18

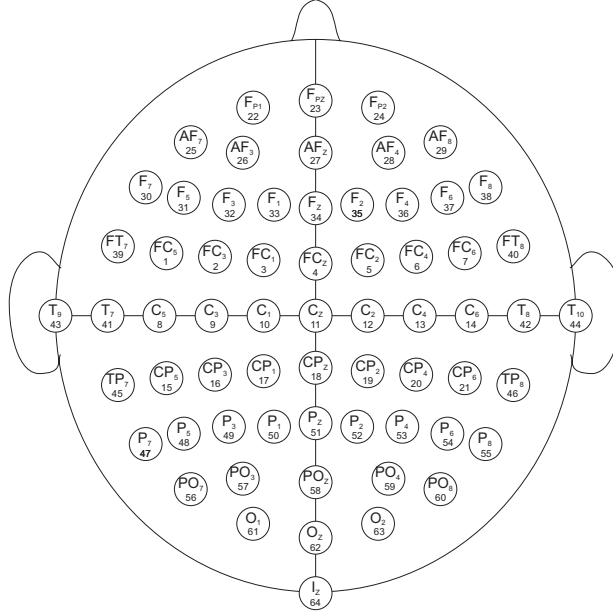


Figure 18: EEG channel configuration labeling (International 10-10 system)

**Preprocessing** This section details the preprocessing steps taken to bring the PCL dataset from its raw form to its final form used in WOODS. The raw PCL dataset contains data from 2 machines, PhysionetMI and Cho17 both used a BCI2000 system [93] while Lee2019\_MI used an undefined machine. Both machines have different channels and sampling frequency characteristics. We take only the 48 channels they have in common and we resample the data to a standard sampling frequency of 250Hz for both machines. We then apply a bandpass filter from 0.3Hz to 30Hz. This bandpass filter removes frequency bands generally regarded as uninformative for the motor imagery task. Finally, we then detrend the data and normalize the data with a standard scaler applied to the channels individually.

**Domain information** The data from the different machines consists of data from disjoint sets of participants. Table 25 details the number of participants per domain and some demographic information; we put N/A for demographic information unavailable work. Table 26 details the proportion of samples and labels across domains.

Domain	Number of participants	Male	Female	Age
PhysionetMI	109	N/A	N/A	N/A
Cho2017	52	33	19	$24.8 \pm 3.9$
Lee2019_MI	54	29	25	[24,35]
<b>Total</b>	215	N/A	N/A	N/A

Table 25: Number of participants and demographic information of the PCL Dataset

Domain	Left Hand	Right Hand	Domain Total
PhysionetMI	2480	2438	4918
Cho2017	4940	4940	9880
Lee2019	3900	3900	7800
<b>Total</b>	11320	11278	22598

Table 26: Domain proportions of labels in the PCL Dataset

**Architecture choice** For this dataset, we use a deep convolution network model as defined in work from Lawhern et al. [56]. We use the implementation of the BrainDecode Schirrmester et al. [94] Toolbox. We chose this model because it is well recognized by the EEG community. It also has a smaller architecture that better fits the data amount and task complexity of the PCL dataset.

### A.5.2 Detailed results

In this section, we detail the results obtained by our baseline algorithms (see Section 7).

**ID evaluation** We show the ID results of ERM for the PCL datasets in Table 27. We obtain these results by doing a hyperparameter search with the methodology detailed in Appendix D, but with no held-out test domain. In other words, all the domains are ID. We then perform train-domain validation to choose the best performing model and report its accuracy.

Algorithm	PhysionetMI	Cho2017	Lee2019 MI	Average
ID ERM	$76.40 \pm 0.19$	$68.07 \pm 0.09$	$76.45 \pm 0.23$	73.64

Table 27: ID results for the PCL dataset

**Baseline evaluation** We show the results of our set of baseline algorithms on the PCL dataset in Table 28. We obtain these results taking every domain as a held-out test set and performing a hyperparameter search with the methodology detailed in Appendix D. Hence, each column of Table 28 corresponds to the domain performance when taken as a test set.

Train-domain validation				
Objective	PhysionetMI	Cho2017	Lee2019 MI	Average
ID ERM	76.40 $\pm$ 0.19	68.07 $\pm$ 0.09	76.45 $\pm$ 0.23	73.64
ERM	63.66 $\pm$ 0.05	59.73 $\pm$ 0.44	70.75 $\pm$ 0.31	64.71
IRM	62.78 $\pm$ 0.80	60.44 $\pm$ 0.75	67.90 $\pm$ 1.02	63.71
VREx	62.53 $\pm$ 0.54	60.13 $\pm$ 0.79	67.77 $\pm$ 1.04	63.48
IB-ERM	63.31 $\pm$ 0.16	59.82 $\pm$ 0.38	70.18 $\pm$ 0.41	64.44
SD	63.72 $\pm$ 0.20	59.31 $\pm$ 0.36	70.15 $\pm$ 0.16	64.40
Oracle train-domain validation				
Objective	PhysionetMI	Cho2017	Lee2019 MI	Average
ID ERM	76.40 $\pm$ 0.19	68.07 $\pm$ 0.09	76.45 $\pm$ 0.23	73.64
ERM	64.02 $\pm$ 0.09	60.51 $\pm$ 0.31	71.04 $\pm$ 0.11	65.19
IRM	63.27 $\pm$ 0.58	60.67 $\pm$ 0.87	67.90 $\pm$ 1.02	63.95
VREx	63.29 $\pm$ 0.18	60.90 $\pm$ 0.63	67.90 $\pm$ 0.95	64.03
IB-ERM	64.63 $\pm$ 0.22	60.22 $\pm$ 0.38	70.27 $\pm$ 0.34	65.04
SD	64.50 $\pm$ 0.05	60.80 $\pm$ 0.17	70.72 $\pm$ 0.14	65.34

Table 28: Baseline results for the PCL dataset

### A.5.3 Credit and license

This dataset is built from 3 different motor imagery datasets [93, 19, 58] as made available on the online MOABB [45] platform. The PhysionetMI dataset is licensed under the Open Data Commons Attribution license v1.0.

## A.6 LSA64

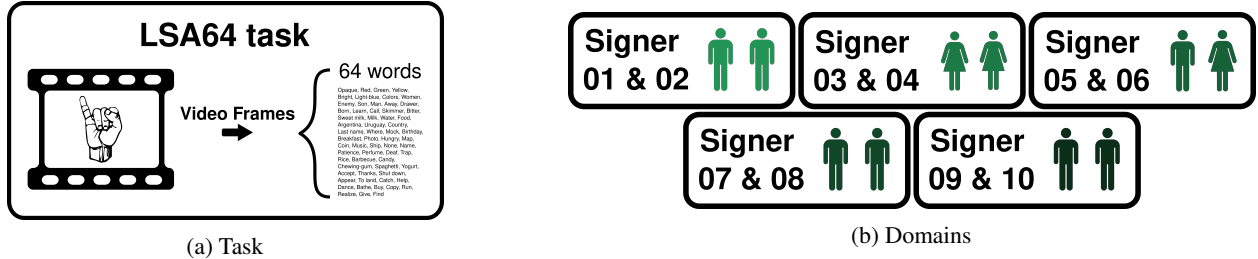


Figure 19: Description of the LSA64 dataset

### A.6.1 Setup

**Motivation** Communication is an idiosyncratic way to convey information through different media: text, speech, body language, and many others. However, some media are more distinctive and challenging than others. For example, text communication has less interindividual variability than body language or speech. If deep learning systems hope to interact with humans effectively, models need to generalize to previously unseen mannerisms, accents, and other subtle variations in communication that significantly impact the meaning of the message conveyed. We study the ability of models to recognize information coming from unseen individuals in the LSA64 dataset.

**Problem setting** We consider the video classification of signed words in Argentinian Sign Language. The labels are a dictionary of 64 words. The dataset consists of ten different signers making multiple repetitions of all 64 words. From that, we create five Source-domains consisting of two speakers each. The goal is to generalize to unseen signers. As a whole, the dataset is composed of 3200 videos of two and a half seconds each at a resolution of (3,224,224).

**Data** The dataset consists of 3200 videos from 10 different signers signing in Argentinian Sign Language. Concretely, the inputs  $x$  are videos of 20 frames of three 224x224 channels. Sequences are about one second long. Domains  $d$  consist of five sets of two signers: Signer 1 & 2, Signer 3 & 4, Signer 5 & 6, Signer 7 & 8, Signer 9 & 10. The labels  $y$  consist of 64 words: Opaque, Red, Green, Yellow, Bright, Light-blue, Colors, Light-red Women, Enemy, Son, Man, Away, Drawer, Born, learn, Call, Skimmer, Bitter, Sweet milk, Milk, Water, Food, Argentina, Uruguay, Country, Last name, Where, Mock, Birthday, Breakfast, Photo, Hungry, Map, Coin, Music, Ship, None, Name, Patience, Perfume, Deaf, Trap, Rice, Barbecue, Cady, Chewing-gum, Spaghetti, Yogurt, accept, Thanks, Shut down, Appear, To land, Catch, Help, Dance, Bathe, Buy, Copy, Run, Realize, Give, and Find.

**Preprocessing** This section details the preprocessing steps taken to bring the LSA64 dataset from its raw form to its final form used in WOODS. The raw LSA64 dataset contains 3200 videos, each about 3 seconds long with the resolution of 1920x1080, at 60 frames per second. We first crop all videos at precisely 2.5 seconds to have videos of the same length. This cropping does not impact the information content of the video as signers pause at the end of their signed words. We then resize the frames to 224x224. Finally, we use PyTorchVideo [25] to uniformly sample 20 frames from each video in a sequence for prediction.

**Domain information** Table 29 details the proportion of samples and labels across domains.

Domain	Words	Domain Total
Signer 1 & 2	10 repetition per word	640
Signer 3 & 4	10 repetition per word	640
Signer 5 & 6	10 repetition per word	640
Signer 7 & 8	10 repetition per word	640
Signer 9 & 10	10 repetition per word	640
<b>Total</b>	50	3200

Table 29: Domain proportions of labels in the LSA64 Dataset

**Architecture choice** We use a Convolutional Recurrent Neural Network (CRNN) for this dataset. The CRNN model has 4 model blocks: Convolutional, Recurrent, attention, and prediction. First, we feed each video frame through a frozen Resnet50 model that is pretrained on Imagenet to extract relevant features. We then feed these feature vectors sequentially to an LSTM model. Finally, push the output of the LSTM model for each frame through a self-attention layer which linearly combines the LSTM output weighed by their attention scores. We then use a fully connected network to make predictions. Table 30 details the layers of the model architecture.

#	Layer
1	Resnet50(in=3x224x224, out=2048)
2	Linear(in=2048, out=512)
3	ReLU
4	BatchNorm(num_features=512, momentum=0.01)
5	Linear(in=512, out=512)
6	ReLU
7	BatchNorm(num_features=512, momentum=0.01)
8	Linear(in=512, out=216)
9	ReLU
10	LSTM(in=256, hidden_size=128, num_layers=2)
11	SelfAttention(in=128, out=128)
12	Linear(in=128, out=64)
13	ReLU
14	Linear(in=64, out=64)

Table 30: Model architecture used for the LSA64 dataset

### A.6.2 Detailed Results

**ID evaluation** We show the ID results of ERM for the LSA64 dataset in Table 31. We obtain these results by doing a hyperparameter search with the methodology detailed in Appendix D, but with no held-out test domain. In other words, all the domains are ID. We then perform train-domain validation to choose the best performing model and report its accuracy.

Algorithm	Speaker 1 & 2	Speaker 3 & 4	Speaker 5 & 6	Speaker 7 & 8	Speaker 9 & 10	Average
ID ERM	$90.10 \pm 0.56$	$89.58 \pm 1.13$	$80.21 \pm 1.06$	$85.16 \pm 1.61$	$87.76 \pm 0.77$	86.56

Table 31: ID results for the LSA64 dataset

**Baseline evaluation** We show the results of our set of baseline algorithms on the LSA64 dataset in Table 32. We obtain these results taking every domain as a held-out test set and performing a hyperparameter search with the methodology detailed in Appendix D. Hence, each column of Table 32 corresponds to the domain performance when taken as a test set.

Train-domain validation						
Objective	Speaker 1 & 2	Speaker 3 & 4	Speaker 5 & 6	Speaker 7 & 8	Speaker 9 & 10	Average
ID ERM	$90.10 \pm 0.56$	$89.58 \pm 1.13$	$80.21 \pm 1.06$	$85.16 \pm 1.61$	$87.76 \pm 0.77$	86.56
ERM	$48.24 \pm 0.51$	$45.51 \pm 0.57$	$41.54 \pm 3.03$	$54.82 \pm 0.60$	$57.29 \pm 1.30$	49.48
IB-ERM	$55.66 \pm 1.71$	$56.71 \pm 2.16$	$49.80 \pm 2.41$	$64.52 \pm 0.61$	$59.70 \pm 2.51$	57.28
IRM	$44.34 \pm 0.60$	$43.16 \pm 1.48$	$38.28 \pm 2.01$	$46.88 \pm 1.13$	$52.47 \pm 2.78$	45.03
SD	$48.63 \pm 2.46$	$50.20 \pm 1.60$	$40.89 \pm 0.84$	$57.68 \pm 2.54$	$56.32 \pm 1.19$	50.74
VREx	$42.19 \pm 3.64$	$42.25 \pm 1.71$	$42.06 \pm 2.82$	$51.82 \pm 1.95$	$52.21 \pm 4.26$	46.11

Oracle train-domain validation						
Objective	Speaker 1 & 2	Speaker 3 & 4	Speaker 5 & 6	Speaker 7 & 8	Speaker 9 & 10	Average
ID ERM	$90.10 \pm 0.56$	$89.58 \pm 1.13$	$80.21 \pm 1.06$	$85.16 \pm 1.61$	$87.76 \pm 0.77$	86.56
ERM	$53.84 \pm 0.28$	$54.23 \pm 0.84$	$49.87 \pm 0.65$	$61.65 \pm 0.46$	$64.52 \pm 0.35$	56.82
IB-ERM	$56.51 \pm 1.38$	$59.51 \pm 0.91$	$51.82 \pm 0.96$	$64.52 \pm 0.61$	$66.54 \pm 1.27$	59.78
IRM	$45.05 \pm 1.13$	$45.25 \pm 1.47$	$39.84 \pm 1.36$	$49.15 \pm 1.69$	$53.12 \pm 2.42$	46.48
SD	$56.58 \pm 1.24$	$60.68 \pm 1.08$	$49.35 \pm 0.51$	$62.43 \pm 0.83$	$64.06 \pm 1.39$	58.62
VREx	$51.24 \pm 0.77$	$50.98 \pm 0.40$	$45.96 \pm 0.46$	$55.21 \pm 0.63$	$58.20 \pm 0.55$	52.32

Table 32: Baseline results for the LSA64 dataset

### A.6.3 Credit and license

This dataset was adapted from the work of Ronchetti et al. [86]. The LSA64 dataset is under the Creative Commons Attribution-NonCommercial-ShareAlike 4.0 International License.

## A.7 HHAR

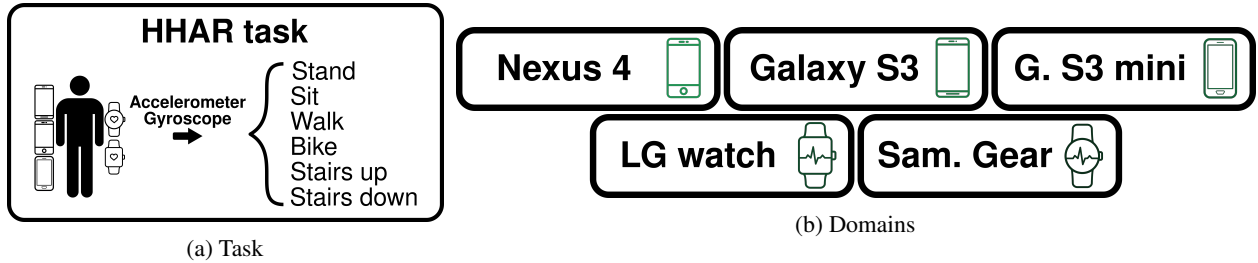


Figure 20: Description of the HHAR dataset

### A.7.1 Setup

**Motivation** Invariant features needed to make predictions in time series are highly convoluted in time with other uninformative features. Because of this, it is a difficult task to extract invariant temporal features from data. We study the ability of models to ignore uninformative information from complex signals with the HHAR dataset.

**Problem setting** We consider the human activity classification task from smart devices (smartphones and smartwatches) sensor data. Sensor data consists of three-axis accelerometer measurements and three-axis gyroscope measurements. The labels are six activities (Stand, Sit, Walk, Bike, Stairs up, and Stairs Down). The data originates from five different devices, which act as our Source-domains. The goal is to find the invariant sensory features across phones and watches. Because watches and cellphones are not worn in the same place on the body, one might have extra oscillations that the model should disregard. As a whole, the dataset is composed of 13674 recordings of five seconds each from six sensor channels.

**Data** The dataset consists of 13674 recordings of 3-axis accelerometer and 3-axis gyroscope data from 5 different smart devices (3 smartphones and 2 smartwatches). Concretely, the inputs  $x$  are recordings of 500 time-steps of a 6-dimensional signal sampled at 100Hz. Sequences are 5 seconds long. Domains  $d$  consist of five smart device models: Nexus 4, Galaxy S3, Galaxy S3 Mini, LG Watch, and Samsung Galaxy Gears. The labels  $y$  consist of 6 activities: Stand, Sit, Walk, Bike, Stairs up, and Stairs Down.

**Preprocessing** This section details the preprocessing steps taken to bring the HHAR dataset from its raw form to its final form used in WOODS. The raw data was gathered with 10 different smart devices (2 from each model: Nexus 4, Galaxy S3, Galaxy S3 Mini, LG Watch, and Samsung Galaxy Gears). Different models have different sampling frequencies, plus recordings have gaps in the data samples where devices temporarily stopped recording, making the time series irregularly sampled. We first remove the recordings of any device that either is missing signals or has less than 100 seconds of recording. We then sort the data points in each sequence according to their recorded time, instead of the indexing created by the devices as the indexing is ordered by the time the data was saved on the device instead of the time of recording. Next, we scale the accelerometer and gyroscope data separately. Finally, we split the full recordings into sequences of five seconds and resample at 100Hz.

**Domain information** Table 33 details the proportion of samples and labels across domains.

Domain	Stand	Sit	Walk	Bike	Stairs up	Stairs down	Domain Total
Nexus 4	760	911	1024	644	695	543	4577
Galaxy S3	664	889	944	560	635	474	4166
Galaxy S3 Mini	409	501	524	297	396	280	2407
LG watch	368	358	382	424	315	307	2154
Gear watch	21	23	78	42	120	86	370
<b>Total</b>	2222	2682	2952	1967	2161	1690	13674

Table 33: Domain proportions of labels in the HHAR Dataset

**Architecture choice** As this data is similar to EEG recordings, we use the same deep convolution network model as in the CAP and SEDFx datasets. The architecture is defined in work from Schirrmeyer et al. [94]. We use the implementation of the BrainDecode Schirrmeyer et al. [94] Toolbox. Temporal Convolutional Networks (TCN) are powerful tools for processing time series data [8]. The architecture we use combines temporal and spatial convolution, which fits this data well. We found that it performed well on this task and obtained solid and stable performance, which is great for our purpose of benchmarking.

### A.7.2 Detailed results

**ID evaluation** We show the ID results of ERM for the HHAR dataset in Table 34. We obtain these results by doing a hyperparameter search with the methodology detailed in Appendix D, but with no held-out test domain. In other words, all domains are ID. We then perform train-domain validation to choose the best performing model and report its accuracy.

Algorithm	Nexus 4	Galaxy S3	Galaxy S3 Mini	LG watch	Sam. Gear	Average
ID ERM	$98.91 \pm 0.24$	$98.44 \pm 0.15$	$98.68 \pm 0.15$	$90.08 \pm 0.28$	$80.63 \pm 1.33$	93.35

Table 34: ID results for the HHAR dataset

**Baseline evaluation** We show the results of our set of baseline algorithms on the HHAR dataset in Table 35. We obtain these results taking every domain as a held-out test set and performing a hyperparameter search with the methodology detailed in Appendix D. Hence, each column of Table 35 corresponds to the domain performance when taken as a test set.

Train-domain validation						
Objective	Nexus 4	Galaxy S3	Galaxy S3 Mini	LG watch	Sam. Gear	Average
ID ERM	$98.91 \pm 0.24$	$98.44 \pm 0.15$	$98.68 \pm 0.15$	$90.08 \pm 0.28$	$80.63 \pm 1.33$	93.35
ERM	$97.64 \pm 0.15$	$97.64 \pm 0.09$	$92.51 \pm 0.46$	$71.69 \pm 0.14$	$61.94 \pm 1.04$	84.28
IRM	$96.02 \pm 0.17$	$95.75 \pm 0.22$	$89.46 \pm 0.50$	$66.49 \pm 0.94$	$57.66 \pm 0.37$	81.08
VREx	$95.81 \pm 0.50$	$95.92 \pm 0.23$	$90.72 \pm 0.10$	$69.04 \pm 0.23$	$56.42 \pm 1.57$	81.58
IB-ERM	$97.56 \pm 0.06$	$97.93 \pm 0.21$	$91.76 \pm 0.57$	$71.38 \pm 1.02$	$59.01 \pm 1.86$	83.53
SD	$98.14 \pm 0.01$	$98.32 \pm 0.19$	$92.71 \pm 0.09$	$75.12 \pm 0.18$	$63.85 \pm 0.28$	85.63
Oracle train-domain validation						
Objective	Nexus 4	Galaxy S3	Galaxy S3 Mini	LG watch	Sam. Gear	Average
ID ERM	$98.91 \pm 0.24$	$98.44 \pm 0.15$	$98.68 \pm 0.15$	$90.08 \pm 0.28$	$80.63 \pm 1.33$	93.35
ERM	$97.98 \pm 0.02$	$97.92 \pm 0.05$	$93.09 \pm 0.15$	$71.96 \pm 0.04$	$64.08 \pm 0.66$	85.01
IRM	$96.02 \pm 0.17$	$95.75 \pm 0.22$	$89.91 \pm 0.25$	$68.00 \pm 0.34$	$57.77 \pm 0.42$	81.49
VREx	$96.65 \pm 0.18$	$96.30 \pm 0.05$	$90.98 \pm 0.16$	$69.39 \pm 0.27$	$59.12 \pm 0.80$	82.49
IB-ERM	$98.16 \pm 0.09$	$98.22 \pm 0.09$	$93.18 \pm 0.16$	$73.40 \pm 0.68$	$64.64 \pm 0.09$	85.52
SD	$98.48 \pm 0.01$	$98.67 \pm 0.11$	$94.36 \pm 0.24$	$75.12 \pm 0.18$	$64.86 \pm 0.28$	86.30

Table 35: Baseline results for the HHAR dataset

### A.7.3 Credits and license

This dataset was adapted from the work of Stisen et al. [102] as made available on the online UCI Machine Learning Repository [23]. This dataset is licensed under the Open Data Commons Attribution license v1.0.



## B Further details on OOD generalization gaps

This section discusses the multiple ways of defining the ID performance and which is the best for measuring attainable generalization gaps. As mentioned in Section 6, the generalization gap is the difference between the performances of a model on data drawn ID and OOD of its training distribution. The *OOD performance* is obtained by training a model on the training domains  $D^{\text{train}}$  with ERM and measure the performance of this model on the test domain  $D^{\text{test}}$ . The ID performance, however, can be defined in different ways. Koh et al. [51] provides multiple definitions for it:

- **Train-to-train** Performance of a model on  $D^{\text{train}}$  when trained on  $D^{\text{train}}$
- **Mixed-to-test** Performance of a model on  $D^{\text{test}}$  when trained on a mixture of  $D^{\text{train}}$  and  $D^{\text{train}}$ .
- **Test-to-test** Performance of a model on  $D^{\text{test}}$  when trained on  $D^{\text{test}}$

In this list, we think that the measure that gives the best measure for achievable generalization gaps is the mixed-to-test because Test-to-test and Train-to-train can lead to erroneous measures.

To illustrate this problem, we explain how the train-to-train measures in the Spurious-Fourier dataset lead to an inflated generalization gap that are unattainable in reality. In the Spurious-Fourier dataset, performing ERM on the training domains  $D^d|_{d \in \{80\%, 90\%\}}$  will lead to models relying on the spurious features to make predictions, as they are a stronger predictor of the label (85%) than the invariant features (75%). Thus, the model will achieve 85% accuracy on data sampled ID to domains  $d \in \{80\%, 90\%\}$ , but only achieve 10% accuracy on the test domain  $D^{10\%}$ . Comparing the ID and OOD performance would lead to a generalization gap of 75%. However, this gap is misleading as a model could never achieve 85% accuracy on the test domain because the strongest invariant predictor can only achieve 75%. A similar case can be made for the test-to-test measure of ID performance, where the generalization gap can lead to an unattainable performance on the test domain.

Instead, let us go through the same example with the mixed-to-test ID performance. Performing ERM on the training domains  $D^d|_{d \in \{80\%, 90\%\}}$  will lead to a predictor that relies on the invariant features, as they are a stronger predictor of the label (75%) than the spurious features (60%). Therefore, the ID performance will be 75%, and the OOD performance will be 10%, leading to a generalization gap of 65%. This gap is a much more significant measure of the upper bound of the performance than the original definition, as it is an attainable gap.

## C Evaluating OOD performance

In theory, the OOD performance of an algorithm is its performance on the test domains  $d \in \mathcal{E}_{\text{all}}$  when trained on a set of training domains  $d \in \mathcal{E}_{\text{train}}$  (see Problem 3.1). In practice, however, a dataset only has a finite number of domains. Thus, a perfect measure of performance on  $\mathcal{E}_{\text{all}}$  is impossible. Instead, we estimate the OOD performance of an algorithm by either performing a

- **Single measure**, where we train an algorithm on a set of training domains, then evaluate on a held-out test domain, or a
- **Cross-validation measure**, where take the average of the single measure for every domain as the test domain.

Both of these approaches are used in the literature: Koh et al. [51] uses a single measure in WILDS, while Gulrajani and Lopez-Paz [29] uses the cross-validation measure in DomainBed. In this work we use the cross-validation measure for our dataset as we think it is a more representative estimation of the performance of an algorithm on test domains  $d \in \mathcal{E}_{\text{all}}$ .

## D Evaluation framework workflow

In this section of the appendix, we detail the methodology employed to evaluate the performance of OOD algorithms on our datasets. For the most part, we follow the workflow used by Gulrajani and Lopez-Paz [29] in their DomainBed testbed.

**Domain cross validation** To get a complete evaluation of the performance of an algorithm on a given dataset, we perform a domain cross-validation measure. We motivate this choice in Appendix C. In summary, for every domain in a dataset, we hold this domain out as the test domain and perform an hyperparameter search by training on the remaining domain. After this hyperparameter search, we perform the model selection associated with the dataset (see Section 8.1) in order to choose a model given a specific validation set. We then report the performance of the chosen model on the

test set. All datasets in WOODS consist of at least 3 domains, therefore there are always at least 2 domains on which to apply an invariance penalty when doing the cross validation.

**Hyperparameter search** For every held-out domain in our domain cross validation, we perform a random search [12] over the hyperparameter distribution of both training and algorithm hyperparameter distribution (see Appendix E) search following the random search. We train 20 models using randomly sampled hyperparameters. We then perform the dataset appropriate model selection methods to select the best models. For each domain, we split the data into 80% and 20% disjoint subsets of the full domain data. We use the 80% split to train the models, and we use the 20% split to validate ID on the training data and perform model selection.

**Statistically relevant** We repeat each hyperparameter search three times to obtain statistically relevant results. This reduces the probability that some algorithm samples a lucky configuration of hyper parameters. All the results reported in this work are averaged over those three hyperparameter trials, we provide the estimated standard deviation of those mean values.

**Reducing bias** The search range is an important topic when discussing the fairness of this evaluation strategy. Having reasonable hyperparameter distributions for sampling in the random search is essential to remaining fair between the algorithms and reducing the induced bias in the results. Defining a narrow hyperparameter distribution for which one knows the algorithm performs very well on a dataset or test domain leads to a bias of the evaluation due to queries of the testing domain under human intervention. This bias could lead to algorithms getting better results by increasing the chance of the random search finding a good value. When defining the hyperparameter range, one should define a range wide enough as to cover the relevant search space for this hyperparameter.

## E Hyperparameter searches

We split the hyperparameter values into 2 categories.

**Training hyperparameters** First, there are training hyperparameters that are functions of the dataset we are training on. They are the base hyperparameters that ERM would need to train. We show the Random distribution used to perform the random search in Table 36.

**Algorithm hyperparameters** Second, there are algorithm hyperparameters that are part of the algorithm definition.

Dataset	Hyperparameter	Random distribution
Spurious-Fourier	learning rate	$10^{\text{Uniform}(-4.5, -2.5)}$
	batch size	$2^{\text{Uniform}(3, 9)}$
	class balance	True
	weight decay	0
TCMNIST-Source	learning rate	$10^{\text{Uniform}(-4.5, -2.5)}$
	batch size	$2^{\text{Uniform}(3, 9)}$
	class balance	True
	weight decay	0
TCMNIST-Time	learning rate	$10^{\text{Uniform}(-4.5, -2.5)}$
	batch size	$2^{\text{Uniform}(3, 9)}$
	class balance	True
	weight decay	0
CAP	learning rate	$10^{\text{Uniform}(-5, -3)}$
	batch size	$2^{\text{Uniform}(3, 4)}$
	class balance	True
	weight decay	0
SEDFx	learning rate	$10^{\text{Uniform}(-5, -3)}$
	batch size	$2^{\text{Uniform}(3, 4)}$
	class balance	True
	weight decay	0
PCL	learning rate	$10^{\text{Uniform}(-5, -3)}$
	batch size	$2^{\text{Uniform}(3, 5)}$
	class balance	True
	weight decay	0
LSA64	learning rate	$10^{\text{Uniform}(-5, -3)}$
	batch size	$2^{\text{Uniform}(3, 4)}$
	class balance	True
	weight decay	0
HHAR	learning rate	$10^{\text{Uniform}(-4, -2)}$
	batch size	$2^{\text{Uniform}(3, 4)}$
	class balance	True
	weight decay	0

Table 36: Distribution range of training hyperparameters for random search

Dataset	Hyperparameter	Random distribution
Invariant Risk Minimization	penalty weight	$10^{\text{Uniform}(-1, 5)}$
	annealing iterations	$\text{Uniform}(0, 2000)$
Variational REx	penalty weight	$10^{\text{Uniform}(-1, 5)}$
	annealing iterations	$\text{Uniform}(0, 2000)$
Spectral Decoupling	penalty weight	$10^{\text{Uniform}(-5, -1)}$
IB-ERM	IB penalty weight	$10^{\text{Uniform}(-3, 0)}$

Table 37: Distribution range of algorithm hyperparameters for random search